BIOCHEMISTRY
including biophysical chemistry & molecular biology

ARTICLE

pubs.acs.org/biochemistry

The Natural Resistance-Associated Macrophage Protein from the Protozoan Parasite *Perkinsus marinus* Mediates Iron Uptake

Zhuoer Lin,[†] José-Antonio Fernández-Robledo,[†] Mathieu F. M. Cellier,[‡] and Gerardo R. Vasta*[,†]

[†]Department of Microbiology and Immunology, University of Maryland School of Medicine, IMET, 701 East Pratt Street, Suite 236, Baltimore, Maryland 21202-3101, United States

[‡]INRS-Institut Armand-Frappier, 531 Bd. des Prairies, Laval, QC, Canada H7 V 1B7

Supporting Information

ABSTRACT: Microbial pathogens succeed in acquiring essential metals such as iron and manganese despite their limited availability because of the host's immune response. The eukaryotic natural resistance-associated macrophage proteins mediate uptake of divalent metals and, during infection, may compete directly for metal acquisition with the pathogens' transporters. In this study, we characterize the *Nramp* gene family of *Perkinsus marinus*, an intracellular parasite of the eastern oyster, and through yeast complementation, we demonstrate for the first time for a protozoan parasite that Nramp imports environmental Fe. Three *PmNramp* isogenes differ in their exon−intron structures and encode transcripts that display a trans splicing leader at the 5′ end. The protein sequences share conserved properties predicted for the Nramp/Solute carrier 11 (Slc11) family, such as 12-transmembrane segment (TMS) topology (N- and C-termini cytoplasmic) and preferential conservation of four TMS predicted to form a pseudosymmetric proton/metal symport pathway. Yeast *fet3fet4* mutant complementation assays showed iron transport activity for PmNramp1 and a fusion chimera of the PmNramp3 hydrophobic core and PmNramp1 N- and C-termini. PmNramp1 site-directed mutagenesis demonstrated that Slc11 invariant and predicted pseudosymmetric motifs (TMS1 Asp-Pro-Gly and TMS6 Met-Pro-His) are key for transport function. PmNramp1 TMS1 mutants D76E, G78A, and D76E/G78A prevented membrane protein expression, while TMS6 M250A, H252Y, and M250A/H252Y specifically abrogated Fe uptake; the TMS6 H252Y mutation also correlates with divergence from Nramp specificity for divalent metals.

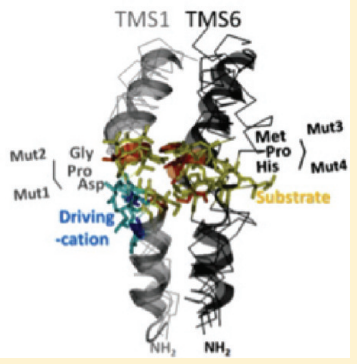

Perkinsus marinus is an intracellular parasite that infects the eastern oyster *Crassostrea virginica* and has caused extensive damage to natural and farm-raised oyster populations along the Atlantic and Gulf coasts of the United States.[1] The life cycle of *P. marinus* includes a free-living stage (zoospore) and a nonmotile vegetative stage (trophozoite). Upon entering the host, most commonly by ingestion during filter-feeding, trophozoites are phagocytosed by oyster hemocytes where they are able to survive and proliferate inside a phagosome-like structure. Although the infection mechanism has not been fully elucidated, a galectin with a unique structure plays a significant role in the entry of the parasite into the host hemocytes.[2] Migration of infected hemocytes throughout the host tissues leads to systemic infection and eventually death.[3] In the environment, transmission of *P. marinus* between oysters likely occurs when released trophozoites from infected oysters are ingested during filter-feeding by adjacent individuals. Over the past 10−15 years, the range of *P. marinus* infection has extended along the Atlantic coast from New Jersey to Maine.[4,5]

Like most intracellular pathogens, *P. marinus* must acquire from the host trace elements such as iron for growth, DNA synthesis, electron transport, energy metabolism, and enzyme activity.[6] The intensity and prevalence of *P. marinus* infections in natural and farmed oyster populations show seasonal trends, mostly associated with water temperature and salinity and metal contaminant levels.[7] Experiments in which oysters maintained in aquaria under various iron concentrations are exposed to *P. marinus* show that higher environmental iron levels lead to increases in *P. marinus* infection intensity.[8] Further, proliferation of in vitro-cultured *P. marinus* is significantly inhibited by chelation of exogenous iron with desferrioxamine (DFO) and can be restored by addition of soluble iron.[9] Taken together, the environmental and experimental evidence strongly suggests that iron uptake is a critical factor for *P. marinus* proliferation and infectivity.[9] Further, the parasite is endowed with effective mechanisms that prevent oxidative damage by either inhibiting the phagocytic respiratory burst or catalytically degrading or scavenging its products,[10−12] which allows its intracellular survival and proliferation.[13] These mechanisms are likely mediated by superoxide dismutases (PmSOD1 and PmSOD2)[14−18] and additional activities of the parasite's antioxidative machinery, including acid phosphatases and ascorbate-dependent peroxidases.[5,16] It is noteworthy that the enzymatic activity of both PmSOD1 and PmSOD2 requires iron as a cofactor,[16] and expression of PmSOD1

Received: March 8, 2011
Revised: June 10, 2011
Published: June 10, 2011

is strongly upregulated as a response to iron starvation, whereas PmSOD2 remains at constant levels.[19] Thus, it is clear that in *P. marinus* iron modulates proliferation, and expression and enzymatic activity of selected virulence factors, although the mechanism(s) for uptake of iron by the parasite has remained unknown.

Iron is considered as a critical factor that contributes to the virulence of microbial pathogens and parasites, and substantial effort has been spent on the identification and characterization of their iron acquisition pathways.[6] Among these, a putative divalent cation membrane transporter that may be responsible for iron uptake was identified as Nramp/Slc11 [natural resistance-associated macrophage protein or solute carrier 11 (recently reviewed in ref 20)]. The Nramp/Slc11 family has ancient origins, and the prokaryotic and eukaryotic functional homologues identified display remarkable sequence conservation, >30% identical along an ~400-amino acid hydrophobic core spanning transmembrane segments (TMS) 1−10.[21] This structural preservation underlies functional conservation as both animal or plant Nramp and prokaryotic homologues (proton-dependent Mn^{2+} transporters, MntH) were reported to complement yeast mutants in *Smf* genes (known as suppressors of the *mif* mutation; *Slc11* homologues) for uptake of divalent metal ions, essentially Mn^{2+}, Fe^{2+}, Co^{2+}, Cd^{2+}, Ni^{2+}, and Cu^{2+}.[22]

Nramp1 is a critical factor in mouse innate resistance to infection by *Mycobacterium bovis*, *Leishmania donovani*, and *Salmonella enterica* serovar *Typhimurium*, three taxonomically distant intracellular pathogens. Although these microbes use diverse mechanisms to survive their host's immune responses, they all rely on acquiring iron for growth and effective antioxidant defense, thus making Nramp1 a highly promising marker for resistance to intracellular pathogens.[20] It is now generally accepted that Nramp1's prime role as a first line of eukaryotic defense is to limit the availability of essential metals within phagocytic vacuoles, using the energy stored in the electrochemical gradient of the proton (acidic phagosome, positive inside) to efflux divalent metals.[23] However, the impact of Nramp1 activity on the maturation of the phagosome depends also on the type of ingested microbe. For instance, both *Dictyostelium discoideum* archetype Nramp and mouse Nramp1 antagonize the *Mycobacterium avium* strategy for intramacrophage parasitism, and Nramp1 activity correlates with a lower phagosomal pH and an increased level of recruitment of the late endosome-lysosome marker Lamp1.[24] In contrast, an active Nramp1 protein in the membrane of *Salmonella*-containing vacuoles enhanced their accessibility both to endosomal vesicles containing fluid phase markers and to M6PR delivery without affecting the phagosomal pH.[24] On the other hand, in *Leishmania*, LIT1 transports Fe^{2+}, and it is required for the replication of the amastigote stage within the host macrophage.[25]

Conversely, the role of bacterial Nramp homologues (MntH) in virulence can vary depending on other factors: both MntH and SitABCD systems facilitate *S. typhimurium* Mn and Fe uptake and contribute to virulence in *Nramp1*$^{-/-}$ and in *Nramp1*$^{+/}$ hosts;[26] *Mycobacterium tuberculosis mntH* is dispensable in a murine model of infection,[27,28] whereas the sole Mn importer of *Brucella abortus* known so far, an *mntH* homologue, is critical for virulence in *Nramp1*$^{-/-}$ mice.[29] In unicellular eukaryotes, the contribution of the iron transporter (LIT1, a cation diffusion facilitator) to *Leishmania* virulence in *Nramp1*$^{-/-}$ mice has been established; otherwise, very limited information is available about the potential role of Nramp transporters from protozoan parasites in infectious pathogenesis.

In a previous study, we identified an Nramp homologue in *P. marinus*, which we designated PmNramp,[30] the first report for any member of the alveolates. In this study, we identify and characterize two novel PmNramp isotypes (PmNramp2 and PmNramp3) and compare their gene organizations, phylogenetic relationships, and evolutionary aspects to those of the initially reported PmNramp1. Further, we examine mechanistic aspects of iron transport activity of PmNramps by yeast complementation, construction of chimeric PmNramp species, and site-targeted mutagenesis, thereby validating a structural basis for transport function that was predicted by homology modeling. Given the key phylogenetic position of *P. marinus* within the Alveolata,[31] this study contributes novel insight into the mechanisms of metal acquisition in protozoan parasites in general and apicomplexans in particular.

EXPERIMENTAL PROCEDURES

***P. marinus* Cultures.** *P. marinus* strain CB5D4 (ATCC# PRA240)[15] was propagated in *Perkinsus* standard culture medium [Dulbecco modified Eagle's (DME) and Ham's F12 (1:2) with 5% fetal bovine serum (FBS)] as reported previously.[32]

Genome Mining. cDNA and amino acid sequences of PmNramp1[30] were used as a query in the search of potential homologues in the *P. marinus* genomic database of the NCBI trace archive database (http://blast.ncbi.nlm.nih.gov/Blast.cgi?PROGRAM=blastn&BLAST_SPEC=TraceArchive&BLAST_PROGRAMS=megaBlast&PAGE_TYPE=BlastSearch). Two contigs were identified in the JCVI (formerly TIGR) database using BLASTn, or tBLASTn using the BLOSUM62 matrix, and a further BLASTx search in the NCBI (www.ncbi.nlm.nih.gov) database indicated that they included members of the Nramp gene family.

Nucleic Acid Extraction, cDNA Cloning, and Sequencing. Parasite cultures in the exponential phase were centrifuged for 10 min at 500*g* and the pellets used for either total RNA extraction with the RNeasy Mini Kit (Qiagen) or DNA extraction with the QIAamp tissue kit (Qiagen) following the manufacturer's instructions. One microgram of *P. marinus* total RNA was transcribed into cDNA using the GeneRacer Core Kit (Invitrogen) according to the manufacturer's protocol; another microgram of total RNA was used to generate first-strand cDNA as reported previously.[33] On the basis of the partial sequences of the PmNramp homologues obtained from genome mining, gene specific primers [PmNR2f, PmNR2r, PmNR3f, and PmNR3r (Table S1 of the Supporting Information)] were designed using the web-based software Primer3 (http://frodo.wi.mit.edu/) for reverse transcription polymerase chain reaction (RT-PCR). The 5′ and 3′ ends were subsequently obtained by RACE (rapid amplification of cDNA ends) procedures with the GeneRacer Core Kit (Invitrogen). For 3′ RACE, the method described by Borson was also used.[33] The 5′ and 3′ RACE products were cloned into the pGEM-T vector (Promega) and confirmed by DNA sequencing of three independent clones. Finally, to confirm the full-length PmNramp2 and PmNramp3 cDNA sequences, primers were designed to target the predicted 5′ end (Table S1 of the Supporting Information) to amplify the full cDNA by 3′ RACE. Products were cloned and sequenced as described above. All PCRs were performed using High Fidelity *Taq* DNA polymerase (Takara), with the following settings: 94 °C for 5 min and then 35 cycles of 94 °C for 30 s, 50−60 °C for 30 s, and 72 °C for 2−4 min.

Structural Analysis by Homology Modeling. Three-dimensional (3D) structural models for the three PmNramp species

were obtained as previously described[34,35] using either MODELER with consensus restraints or iterative TASSER simulations (I-TASSER).[36] The default parameters used were those of the programs developed by the Zhang laboratory, including the Local Meta-Threading-Server (LOMETS)[36] that generates 3D models by collecting consensus target-to-template alignments from nine locally installed threading programs, and the MUlti-Sources ThreadER (MUSTER)[36] that combines sequence profile−profile alignment with multiple structural information. The Protein Data Bank (PDB) coordinates calculated by the different programs were used to visualize the three-dimensional models using the freeware viewer Pymol (http://www.pymol.org).

Phylogenetic Analysis. To phylotype the three PmNramp, a representative set of eukaryotic homologues was selected to generate multiple alignments using full-length amino acid sequences and Clustal X[37] or Muscle, which were edited manually and used alternatively to compare phylogenies. Sets of parsimony-informative sites (corresponding to at least two different amino acids, and at least two of them occurring with a minimum frequency of 2[38]) were also examined as an alternative to full-length sequences to examine tree robustness. A consensus phylogenetic tree was established by implementing several approaches using different substitution models. The rate of amino acid variation among sites was modeled using the WAG amino acid substitution matrix[39] and a discrete Gamma distribution.[40] Phylogenies were inferred using three different types of calculations: (i) change probabilities along the tree branches determined by Quartet Puzzling and Maximum Likelihood using Tree-Puzzle,[40] (ii) pairwise evolutionary distances (numbers of substitutions) deduced by the Minimum Evolution/Neighbor-Joining method[38] and allowing a heterogeneous pattern of substitution across the lineages[38] as well as pairwise or complete deletion modes,[38] and (iii) maximum parsimony[38] used to deduce the evolutionary transitions required to explain the observed amino acid distributions.[38] The consistency of each calculation was estimated by bootstrapping[38] (3000 replicates), and the confidence score of tree nodes was compared.

To evaluate the type of selective pressure exerted on *Perkinsus* gene sequences, Kumar's modification of the Pamilo−Bianchi−Li method was used to analyze the relative abundance of synonymous (S) and nonsynonymous (N) substitutions in codon-by-codon pairwise comparisons of the three aligned *PmNramp* nucleotide sequences.[38] After the number of synonymous substitutions per synonymous site (d_S) and the number of nonsynonymous substitutions per nonsynonymous site (d_N) as well as their variances, Var(d_S) and Var(d_N), had been estimated, the level of significance at which the null hypothesis of neutral evolution (H_0, $d_N = d_S$) may be rejected was tested considering three alternative hypotheses (AH1, $d_N \neq d_S$, strict neutrality; AH2, $d_N > d_S$, positive selection; AH3, $d_N < d_S$, purifying selection). A two-tailed Z test was used to determine the level of significance of the difference $d_N - d_S$ (AH1), and a one-tailed Z test was applied to examine the other hypotheses (AH2 and AH3). Both pairwise and complete site deletion options were used to compare the results obtained; the variance of the difference $d_N - d_S$ was calculated by bootstrap resampling (3000 replicates).

To visualize how positive and negative evolutionary selection are distributed along PmNramp molecules, we used the BioJava framework-based JCoDA software[41] to scan PmNramp MSA by implementing the d_N/d_S calculation from the Phylogenetic Analysis using Maximum Likelihood (PAML, Codeml[42]) and using a sliding window. To perform site-specific analyses, a ML tree was generated and likelihood ratio tests were conducted using six possible models of nucleotide substitution: M0 and M3 evaluate whether the sequences studied are under identical pressure, while M1, M2, M7, and M8 seek for the presence of purifying, neutral, or positive selection; M1 and M2 use discrete values, while M7 and M8 use a β distribution.[43]

The molecular clock hypothesis was evaluated using Tajima's relative rate test, which implies equality of evolutionary rate between two sequences, irrespective of a substitution model, and whether the substitution rate varies among sites.[38] Pairs of PmNramp nucleotide or amino acid sequences were compared, using the third sequence as the outgroup. Tajima's method uses a χ^2 test to estimate the independence of paired observations on two variables; a value of the corresponding probability ($p < 0.05$) was used to reject the molecular clock hypothesis.

The homogeneity of substitution patterns was derived from pairwise sequence comparisons using the Disparity Index test, which calculates the extent of differences in base or amino acid residue composition between sequences. The probability p of rejecting the null hypothesis that sequences evolved with the same pattern of substitution was determined using a Monte Carlo test and bootstrap resampling (3000 replicates).[38]

Functional Analysis of PmNramp1 in Yeast. *P. marinus* Nramp1 cDNA sequences with a HA tag at the 3′ end were cloned into the *Not*I site of yeast expression vector pFL61. The ferrous iron transport-deficient yeast strain DEY1453 (*fet3fet4*)[44] was transformed using lithium acetate and selected for growth on synthetic-defined (SD) medium (pH 5.6) containing 20 mg/mL glucose and appropriate autotrophic requirements and supplemented with $FeCl_3$ to promote yeast growth.[45] Genomic DNA was extracted from transformed yeast cells using the QIAamp tissue kit (Qiagen) following the manufacturer's instructions. Extracted DNA was used to confirm the existence of the vector by PCR using primer PmNramp1F and pFL61R (Table S2 of the Supporting Information). Total RNA was extracted from the transformed yeast cells with the RNeasy Mini Kit (Qiagen). RT-PCR was performed to examine the expression of PmNramp1 mRNA in yeast. A yeast-enriched membrane fraction was tested via Western blotting for expression of PmNramp1 using the monoclonal anti-HA high-affinity antibody 3F10 conjugated with biotin (Roche Applied Science) and streptavidin-peroxidase (Sigma). Complementation experiments were performed using the methods of Eide and colleagues.[46] The *Arabidopsis thaliana* ferrous iron transporter (AtIRT1),[47] known from previous yeast complementation assays to be an efficient Fe^{2+} transporter,[45] was used as a positive control. As a negative control, yeast was transformed with the pFL61 vector alone.

Construction of Chimeric PmNramp Isotypes. To test the metal transport capacity of PmNramp2 and PmNramp3, their N- and C-termini were swapped with those of PmNramp1. For swapping of N-termini, a *Bam*HI restriction site was introduced by PCR into the coding regions of all three isotypes, using the primers listed in Table S2 of the Supporting Information. To verify that introduction of this restriction site does not perturb PmNramp1 function, PmNramp1 with the *Bam*HI site was included as a control in the yeast complementation assays. For swapping of C-termini, an *MscII* site was identified at the end of TMS12 of PmNramp1 and was introduced into the corresponding positions in PmNramp2 by PCR with the primers listed in Table S2. An *Sph*I site was found in the same proximal region of PmNramp1. For the replacement of the C-terminus of

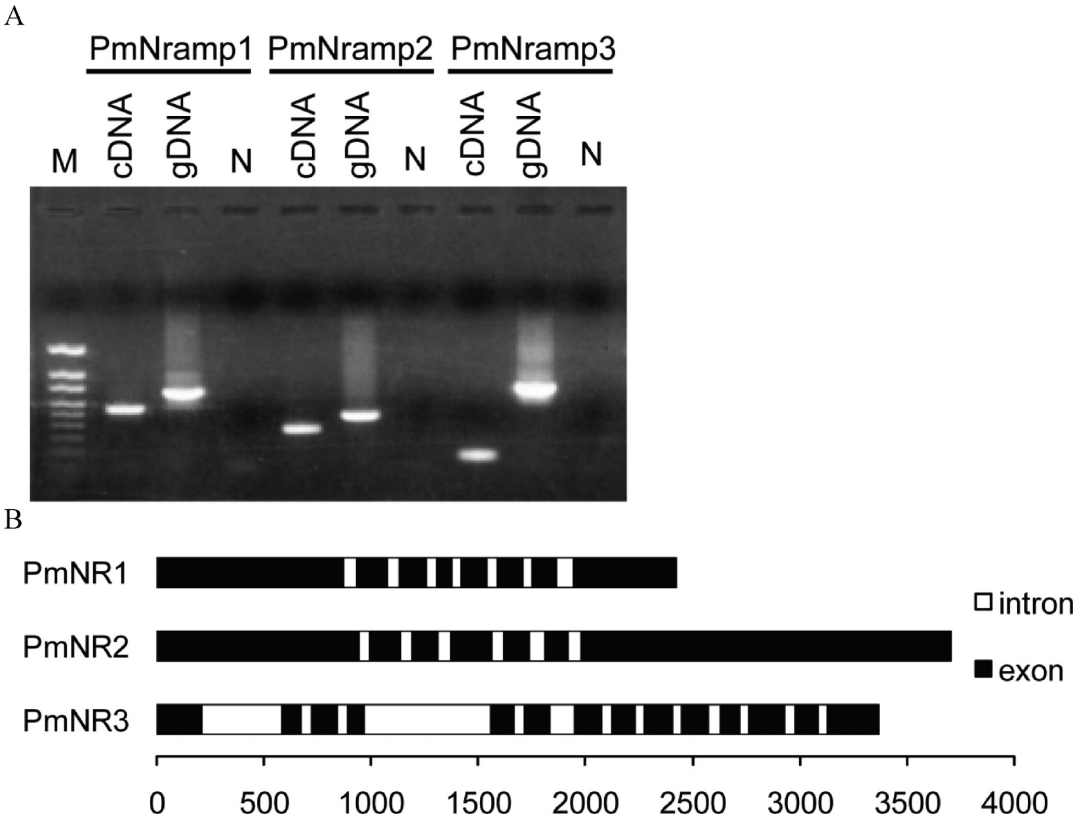

Figure 1. RT-PCR analysis and gene organization of *PmNramp* isotypes. (A) The three *PmNramp* isotypes are all constitutively expressed in trophozoites grown in standard medium. Abbreviations: cDNA, *P. marinus* cDNA; gDNA, *P. marinus* genomic DNA; N, negative control; M, 100−1.5 kb DNA marker. In a 1.2% agarose gel, with ethidium bromide and 1× Tris-acetate-EDTA. (B) Physical organization of the *PmNramp* homologous genes deduced from genomic and cDNA sequence analyses. Exons and introns are indicated with filled and empty boxes, respectively. The *x*-axis indicates the size in base pairs.

PmNramp3, the *Sph*I site was added to the PmNramp3 coding region.

Site-Directed Mutagenesis. To test the structural and functional value of the 3D predicted model and the importance of the canonical tripeptides in TMS1 and TMS6 for PmNramp1 function, selected amino acid residues were mutated by site-directed mutagenesis using QuikChange II Site-Directed kit (Stratagene). The primers used for introducing the mutations are listed in Table S3 of the Supporting Information. All mutations were confirmed by sequencing prior to the yeast complementation assays.

Immunofluorescence Staining of Yeast Cells. *fet3fet4* yeast cells transformed with PmNramp1, PmNramp3, chimeric PmNramp3, and all the PmNramp1 mutants were harvested for immunofluorescence staining. Cells were fixed in 4% formaldehyde in SD medium at room temperature for 30 min, and the cell wall was digested with 50 μg/mL lyticase (Sigma) at 30 °C in 0.1 M potassium phosphate buffer containing 1.2 M sorbitol (pH 7.5) for 5 h. Cells were centrifuged, resuspended in PBS, applied to the slide wells (Thermo Scientific), and allowed to sediment for 40 min. Cells were dehydrated in cold methanol for 6 min at −20 °C, washed in cold acetone (−20 °C) for 10 s, and dried at room temperature. Immunofluorescence studies were performed as follows. Samples were pretreated with 3% PBS-BSA for 1 h at room temperature, followed by incubation with a mouse anti-HA antibody (monoclonal 16B12; Covance) at a 1:100 dilution in 3% PBS-BSA for 1 h at room temperature. After three washes in PBS for 5 min, samples were incubated with a fluorescein isothiocyanate-conjugated goat anti-mouse antibody (Sigma) at a 1:100 dilution in 3% PBS-BSA in the dark for 1 h at room temperature. After three washes in PBS for 5 min, samples were stained with 4′,6-diamidino-2-phenylindole (DAPI) (Invitrogen, Carlsbad, CA) at a 1:1000 dilution in 3% PBS-BSA for 10 min, followed by three washes in PBS. Subsequently, the samples were mounted in the ProLong Gold antifade reagent (Invitrogen), stored in the dark at 4 °C, and examined using a Nikon Eclipse E800 fluorescence microscope, and images were taken with a SPOT RT2540 camera (Diagnostic Instruments, Inc.).

RESULTS AND DISCUSSION

Identification and Characterization of Two Novel PmNramp Isotypes. The number of Nramp isotypes varies substantially from organism to organism (e.g., Table S4 of the Supporting Information). Two archetype Nramps are present in humans and mice, whereas *Saccharomyces cerevisiae* possesses three prototype Nramps. With regard to protozoan parasites, a single potential archetype Nramp was annotated in the genome databases of *Plasmodium* spp. (http://plasmodb.org/plasmo/) and *Toxoplasma gondii* (http://toxodb.org/toxo/). Mining the *P. marinus* genomic databases using the sequence of the *PmNramp* gene that we had previously characterized identified two new contigs encoding potential Nramp homologues. RT-PCR with gene-specific primers targeted to each of these homologues confirmed the presence of their transcripts in *P. marinus* trophozoites cultured in standard medium (Figure 1A), indicating constitutive gene expression in this particular life cycle stage of *P. marinus*.

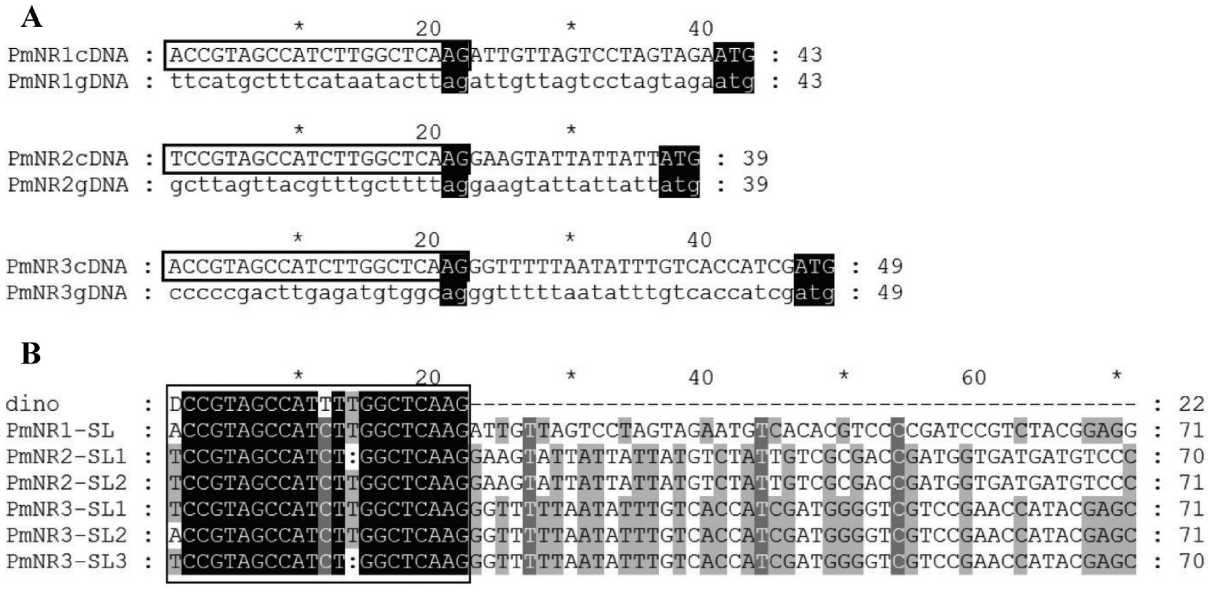

Figure 2. Conserved SL sequence from *P. marinus Nramp* mRNAs. (A) Alignment of the 5′ UTRs of *P. marinus Nramp* cDNAs and corresponding genomic (gDNA) sequence revealing the 22-nucleotide trans spliced splicing leader (SL) marked by a box. (B) Alignment of the 5′ end of *PmNramp* isotype cDNAs. The consensus SL sequence from dinoflagellates is compared with that from *P. marinus*. dino represents the dinoflagellate consensus SL (D = T, A, or G). The 22-nucleotide SL sequence is highlighted by a square box. For PmNramp1-SL, all the SL sequences from three independent clones of *PmNramp1* have the same sequence. For PmNramp2-SL1 and PmNramp2-SL2, two different SL sequences with a deletion in one of them were obtained from three independent clones. For PmNramp3-SL1, PmNramp3-SL2, and PmNramp2-SL3, three SL sequences with either deletion or nucleotide substitution were identified at 5′ ends of *PmNramp3* mRNA.

P. marinus RNA was used to obtain the full-length cDNAs encoded by these novel *Nramp* genes, hereafter designated PmNramp2 (GenBank accession number EU589239) and PmNramp3. The first in-frame initiator methionine codon at position 37 of the *PmNramp2* cDNA sequence was followed by a 1947-nucleotide coding DNA sequence (CDS) encoding a putative protein of 649 amino acid residues with a predicted relative molecular mass of 70.5 kDa. The *PmNramp3* cDNA was 1726 bp long, with a 1677 bp CDS encoding a putative protein of 559 amino acid residues with a predicted relative molecular mass of 60.0 kDa. No canonical polyadenylation signals were identified in *PmNramp2* or *PmNramp3*. Alignment of the cDNA and genomic sequences revealed seven exons interrupted by six introns in *PmNramp2* (Figure 1B). Most of the exon−intron boundaries were characterized by the canonical splicing signal (GT/AG) with the exception of a noncanonical 3′ donor site in *PmNramp2* intron 3 (GT/GC). The translational start codon was within the first exon, and the termination codon (TGA) was located in exon 7, which has a 3′ untranslated region (UTR) more than 1 kb long. *PmNramp3* has 14 exons interrupted by 13 introns, and the start and stop codons are located in the first and last exons, respectively. The exon−intron organization of *PmNramp2* is similar to that of *PmNramp1*, which contains eight exons (Figure 1B), instead of the seven reported in a previous study.[30]

Pairwise amino acid sequence alignment of PmNramp2 and PmNramp3 with human Nramp2 (GenBank accession number BAA24933) and PmNramp1 (GenBank accession number AAQ94879) showed that human Nramp2 is 36, 32, and 34% identical to PmNramp1, PmNramp2, and PmNramp3, respectively. Among the three PmNramp isotypes, PmNramp1 and PmNramp2 display the highest levels of identity in both amino acids (51%) and nucleotides (54%). Such a low level of nucleotide identity (44−54%) among the three isotypes can explain that *PmNramp2* and *PmNramp3* were not detected in Southern blots using PmNramp1 probes at high stringency.[30]

Trans Splicing of PmNramp1−3 mRNAs. No information about regulation of gene expression is yet available for *P. marinus*, and no clear TATA box has been identified in any of the genes characterized to date.[15,16,30] However, the 100 bp upstream of the transcription starting point was enough to drive transcription of *PmMOE*, a gene selected for the development of a *P. marinus* transfection system.[15] The recent report of a trans splicing leader in dinoflagellates also indicated that *P. marinus* and *Perkinsus chesapeaki* cDNAs are trans spliced.[48] In dinoflagellates, nuclear-encoded mRNAs are trans spliced by addition to the 5′ end of a 22-nucleotide conserved splicing leader (SL) of sequence DCCGTAGCCATTTTGGCTCAAG (D = T, A, or G).[48] Analysis of the 5′ cDNA sequences of *PmNramp2* and *PmNramp3* revealed a 20-nucleotide stretch that was absent in the *PmNramp2* and *PmNramp3* genomic vicinities (Figure 2A). Re-examination of the 5′ sequence of *PmNramp1*[30] revealed the same feature (Figure 2A). A fairly good match occurs in the alignment of the 5′ end of the *PmNramp* mRNA with the SL consensus sequence from dinoflagellates (Figure 2B), indicating that the mRNAs of all three *P. marinus Nramp* genes are trans spliced with a conserved SL.

SL trans splicing has been documented in a limited but diverse number of eukaryotes, in which this process makes it possible to translate polycistronically transcribed nuclear genes. Trans splicing has been detected in nematodes, platyhelminths, cnidarians, rotifers, ascidians, appendicularians, and dinoflagellates.[49] In *Trypanosoma* spp., all genes are trans spliced[50] and the SL is a conserved 35-nucleotide stretch. Comparison of genomic DNA and cDNA of *PmNramp* isotypes revealed that at the junction between the SL sequence and the 5′ UTR of *PmNramp*, the genomic DNA sequence bears the dinucleotide AG (Figure 2B),

consistent with the canonical cis and trans splicing acceptor boundary, apparently serving as the acceptor site of SL.[49] In dinoflagellates, a conserved "CGTGTGC" sequence was identified immediately upstream of the 3′ acceptor splice site AG of the genes analyzed.[48] However, no such conserved sequence is found in any of the three *PmNramp* isotypes. Interestingly, the SL sequences from both *PmNramp2* and *PmNramp3* isotypes carry a thymidine deletion at the same position (Figure 2B). The presence of the predicted trans splicing leader in all *PmNramp* cDNAs indicates that these genes may be transcribed polycistronically and constitutively. In *Trypanosoma*, constitutive transcription of all the genes makes RNA interference (RNAi) an important avenue for regulation of the parasite gene expression, as well as a widely used knockdown technique in *Trypanosoma* research.[51] In the *P. marinus* genome databases, some components of the RNAi machinery have been identified by BLAST, indicating possible regulation of constitutive gene expression through RNAi.

All three *PmNramp* isotype mRNAs lack known regulatory nucleotide sequence motifs [e.g., iron responsive element (IRE)] and are detected in trophozoites cultured under standard conditions. Therefore, because *PmNramp* transcript levels did not change under conditions of iron overload, iron depletion, and challenge with oyster serum, we favor the possibility that like other *P. marinus* genes with trans spliced leaders such as *SOD* and *APX* (data not shown), the PmNramp proteins are subject to post-translational regulatory mechanisms. In yeast, the three prototype Nramp isotypes are regulated differently: while the vacuolar iron transporter Smf3 is controlled at the transcriptional level,[52] the manganese transporter Smf1 and Smf2 proteins are constitutively expressed and trafficked to either degradation or secretory pathways depending on manganese availability and the protein Bsd2,[53] following a mechanism reminiscent of Ndfip1-dependent regulation of human Nramp2/DMT1 expression via ubiquitination by Nedd4 family members of the HECT ubiquitin ligase family (E3[54]). Ndfip1 and WWP2 target DMT1 for ubiquitin-dependent degradation similar to Bsd2p/Rsp5p-mediated degradation of Smf1/2p in yeast.[55] The mechanism by which Me^{2+} (Mn or Fe) is sensed through Bsd2p and Ndfip1 remains to be determined.[55] Acquisition of iron and other vital divalent cations is crucial for *P. marinus*, as well as avoiding metal poisoning. Therefore, constitutive expression of PmNramp mRNA either ready for protein synthesis or constitutively translated and regulated post-translationally in a metal-dependent manner would allow an immediate response to metal requirements. Further, on the basis of querying the *P. marinus* genome with *Chlamydomonas reinhardtii* ferritin sequences (GenBank accession numbers AF503338 and EU223296), *P. marinus* may express one or two ferritins, consistent with the ability to metabolize and store the incorporated iron.

Functional Features Predicted from Protein Sequence Structural Modeling Analysis. Genetic studies using prokaryotic and eukaryotic Slc11 homologues and various topological reporters have yielded a consensus transmembrane topology that places both ends of the Slc11 hydrophobic core (TMS1−10) on the cytoplasmic side of the membrane, though some extramembranous loops still remain to be tested experimentally.[35] A multiple-Nramp sequence alignment (Figure 3) shows residue conservation predominantly in the Slc11 hydrophobic core and invariant residues forming clusters in areas corresponding to TMS1−10. This precise structural conservation suggests that like the human equivalents, PmNramps may function as divalent cation transporters.

The predicted Slc11 global transmembrane topology also fits a three-dimensional fold (LeuT or Slc6),[34,56,57] which is conserved among apparently distant families of Na^+- or H^+-dependent transporters showing less than 15% overall amino acid sequence identity (Slc5 or Mhp1 and Slc7).[56,57] Slc11 comparative modeling was initially performed by threading sequences onto the LeuT structure representative of Na^+-coupled amino acid transporters (Slc6), and the *Escherichia coli* MntH model was tested both functionally and topologically using several Slc11-specific mutants.[34] Because a low-level sequence relationship imparts moderate structural accuracy, we searched for indications of the functional significance of the models produced by additional threading using available resources and the ever-expanding RCSB Protein Data Bank (http://www.rcsb.org/). As novel structures determined for members of apparently unrelated families of cation-driven transporters revealed the conservation of the LeuT architecture,[56,57] this approach allowed us to evaluate consistency levels among various Slc11 models in the absence of significant sequence similarity.

The similar structures of transporters Mhp1, LeuT, vSGLT, and ApcT represent discrete steps in a "gated-pore" transport cycle common to diverse families of cation-driven carriers: (1) open to out, (2) open to out and "occluded" by substrate and closure off from external bulk water, and (3) open to in.[56,57] Additional crystal structures indicated that this common architecture was probably not preserved by use of a common cation-motive force for transport, because both Na^+- or H^+-dependent and -independent carriers altogether share the same 3D organization.[56−59] Instead, the presence of equivalent residues that replace a given cation functionally was reported among various structures.[56,57] In fact, such a structurally conserved LeuT fold has been proposed as testimony to the functional importance of the carrier-inverted symmetry, with two five-TMS repeats assembled in antiparallel orientations that place cosubstrate binding sites at the apex of a cavity formed in part by TMS1, -3, -6, and -8. Internal 3D symmetry may have allowed sequence divergence to adapt this scaffold for uptake of various substrates using distinct forms of energy (electrochemical gradients of Na^+, H^+, or other cosubstrates[60]). Indeed, using structure-based sequence alignment and independent phylogenetic and clustering approaches, homology was demonstrated among the families known to share the LeuT fold (Slc5, -6, -7, and -38, NCS1, and BCCT) but not those displaying other structurally inverted symmetries [Clc channels or Amt (Slc42) carriers[61]]. Slc11 carriers also clustered with the LeuT superfamily in these analyses, implying thus remote structural homology.[61]

Fittingly, the two Slc11-specific triplets, Asp-Pro-Gly (TMS1) and Met-Pro-His (TMS6), were predicted to occupy the central position and, together with segments of TMS3 and TMS8, to form part of a three-dimensional arrangement mediating directional cation symport.[56,57] The TMS1 DPG peptide contributes to proton-binding and -motive force, shown by the loss of H^+ uptake in *E. coli* MntH Asp^{34} mutants, while TMS6 residues MPH participate in pH-dependent regulation consistent with the requirement for *E. coli* MntH His^{211} for Cd^{2+} uptake at neutral pH. These two Slc11-invariant sites were accessible in situ to fluorescein-maleimide and *N*-ethylmaleimide, respectively, while three others were not, corresponding to transmembrane Asn residues that could mediate interhelix interactions key for transport.[34] Hence, both the Slc11 global transmembrane topology established using distant relatives and in situ accessibility of Slc11-specific functional residues fit the 3D LeuT fold and support homology inference.

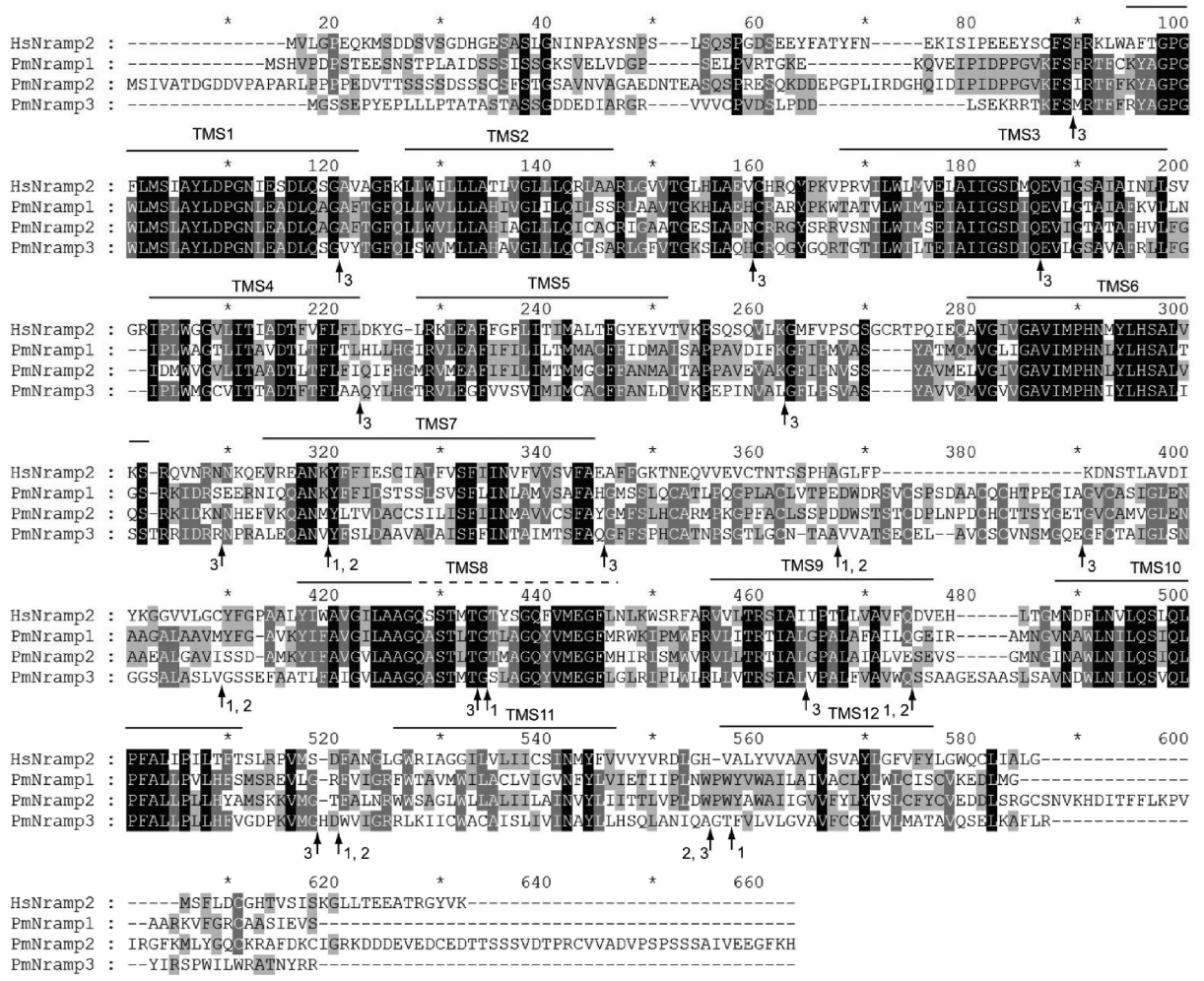

Figure 3. Multiple-sequence alignment of deduced amino acid sequences of PmNramp1, PmNramp2, and PmNramp3 with human Nramp2 (HsNramp2). The alignment was generated using Mega 4.0[38] and displayed with GeneDoc.[83] Identical residues are highlighted at three cutoffs (50, 75, and 100%). The TMS predicted by homologous modeling are spanned by black lines and numbered 1−12. The previously described PmNramp "conserved transport motif", now predicted as part of TMS8, is indicated by a dashed line. Arrows represent the exon boundaries in the protein sequence, with the number indicating corresponding *PmNramp* isotype number.

Moreover, the Slc11 TMS6 His residue from the MPH triplet represents a predicted rate shift upon comparison of the Nramp family either to its outgroup[62] or to the divergent subgroup Nrat1 (Figure S1 of the Supporting Information) recently described in plants.[63] Nrat1 is unable to complement the ferrous iron uptake-deficient yeast strain (*fet3fet4*) because it transports trivalent metals instead of divalent metals.[63] As Nrat1 emerged before diversification of monocots (grasses; http://www.phytozome.net), we could evaluate site-specific sequence divergence;[62,64] likelihood ratio test analyses indicated that all three PmNramps share a conserved pattern of residues that distinguishes bona fide members of the Nramp family (Me^{2+} carriers) from members of the divergent subgroup of Nrat1 that carry Me^{3+}. Nrat1 TMS6 was the most divergent, with two predicted type II rate shifts matching the Nramp functional signature MPH (changed for TPY); TMS1, -3, -5, -7, and -8 also contained sites possibly contributing to Nrat1's functional preference for trivalent cations (Figure S1 of the Supporting Information). More generally, the Nramp versus Nrat1 sequence comparison shows candidate rate-shifted sites in pairs of TMS predicted to be symmetric [TMS1 and TMS6, and TMS3 and TMS8 (Figure S1 of the Supporting Information)] and central to substrate uptake according to LeuT homology modeling.

Figure 4 shows the best models obtained by threading PmNramp1 sequence on available PDB templates, which detail potential alternating conformational states presumed to affect PmNramp1 TMS1, -3, -6, and -8 during metal uptake activity, based on the determined structures of Mhp1 and vSGLT. An open-to-out conformation would allow cation cosubstrates to reach their translocation site, approximately in the middle of the plasma membrane, involving the Slc11-specific residues Asp-Pro-Gly (TMS1) and Met-Pro-His (TMS6) as well as other residues from TMS3 and -8, and possibly also TMS2 and -7. After PmNramp1 isomerization, an open-to-in conformation would allow the release on the other side of the membrane of the driving cation and Me^{2+} substrate. As depicted in Figure 3, clusters of residues invariant among PmNramps are found along these TMS predicted to line the central transmembrane aqueous translocation pathway (TMS1, -3, -6, and -8). By contrast to the divergence of plant Nrat1 toward the Al^{3+} substrate that involved site-specific variations in these TMS (Figure S1 of the Supporting Information), local sequence conservation among PmNramp

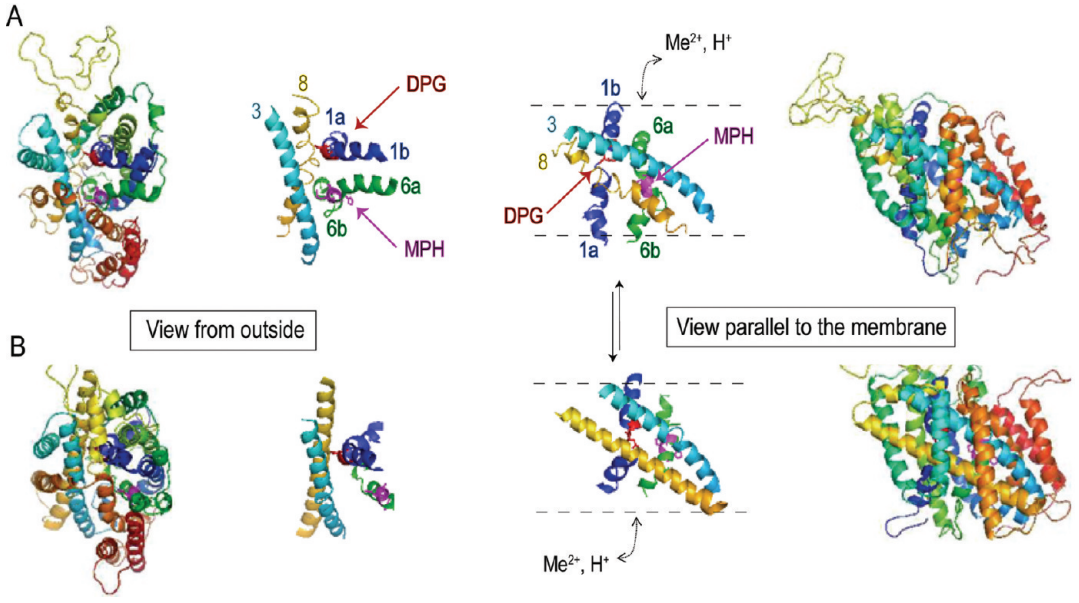

Figure 4. Hypothetical model for transmembrane symport of divalent metals and protons via PmNramp1. A short version of PmNramp1 (Pm1_NCD, 485 residues; ^{58}VKFSF...EDLMG^{542}) was used to generate alignments that mapped PmNramp1 residues to homologous sites on candidate template crystal structures using the algorithm Muster.[36] The models were derived from *Microbacterium liquefaciens* nucleobase-cation symport1 transporter, in an open-to-out conformation (A),[56,57] or from *Vibrio parahemolyticus* sodium/galactose symporter, in an open-to-in conformation (B).[56,57] Two views are presented for each model as indicated, one from the external surface (outside) and one parallel to the membrane with TMS4 and -9 in front (45° and 90° rotations). For each view, either the 485-residue continuous structure is shown or that corresponding only to the residues that constitute TMS1, -3, -6, and -8 is shown. The symmetric extended tripeptides DPG and MPH that connect the half-helices 1a and 1b and half-helices 6a and 6b are colored red and magenta, respectively. A possible pathway of metal and proton symport through alternating access is outlined.

TMS1, -3, -6, and -8 suggests a key functional role in Me^{2+} uptake.

The sequence of the conserved transport motif [indicated with a dashed line (Figure 3)] is now predicted as being integral to TMS8 in the three-dimensional Slc11 model structure obtained by threading.[34,35] Such a conserved transport motif was initially proposed to form a cytoplasmic re-entrant loop, situated immediately downstream of a shorter TMS8, and predicted to contribute to cation selection by analogy with the "pore region" of K^+ channels and glutamate and GABA transporters.[65] This suggestion was re-evaluated because (i) the pore region of the GABA and serotonin transporters corresponds in fact to the TMS8 in LeuT-based models[66,67] and (ii) indeed the GABA transporter pore region was demonstrated experimentally to form a transmembrane helix lining the aqueous translocation pathway.[66] Again, though such TMS8 deduced from LeuT homology modeling showed likely rate-shifted sites in sequence comparisons between Slc11 carriers and members of either its outgroup or the Nrat1 variant subgroup[61] (Figure S1 of the Supporting Information), the high level of sequence conservation observed among PmNramp TMS8 (Figure 3) is consistent with a key functional role in Slc11 Me^{2+} transport.

Sequence divergence among PmNramp homologues corresponds predominantly to regions thought to be extramembranous (Figure 3), which can nevertheless harbor site-specific signals for protein localization and/or turnover. Distinct Lys residues in the yeast Smf1p N-terminal hydrophilic sequence are targeted for Rsp5p-dependent ubiquitination to promote endocytosis in response to external cadmium[68] and to toxic manganese.[69] These observations suggest that divergent sequences among PmNramp extramembranous regions may still contain residues useful for post-translational regulation of expression, subcellular localization, and trafficking of PmNramps in response to environmental metals.

Phylogenetic Analysis. For phylotypes PmNramp2 and PmNramp3, detailed analyses were performed using a set of sequences representative of eukaryotic Nramp diversity (Figure S2 and Table S4 of the Supporting Information). Data were summarized with the linearized phylogenetic tree presented in Figure 5, showing key nodes supported by high bootstrap values obtained with different methods. The *P. marinus* Nramp sequences (PmNramp1−3) form a moderately tight set among other homologues that together constitute Nramp archetype subgroup II.

Phylotyping Slc11 homologues suggests several steps in the evolution of Slc11 function: from remote homology with sodium- or proton-motive substrate symporters to metal nutrition in bacteria (Outgroup > MntH B > MntH A) and to eukaryotic cell defense and functions (MntH A > eukaryotic outparologs: proto-/archetype Nramp) as well as further bacterial adaptation (prototype Nramp > MntH Cα, Cβ, Cγ). Eukaryotic Nramp homologues were found in bikonts (plants and chromoalveolates) and unikonts (amebozoans, fungi, and animals).[30,70] Nramp archetype subgroup I was found only in monocot and eudicot plants, and it contained the ancestor of Nrat1 variants.[63] Prototype Nramps were restricted to amebozoans and fungi, green or red algae, and lower plants, e.g., bryophytes, implying selective loss of this isoform in animals and higher plants, as well as in chromoalveolates. Close relationships between some bacterial MntH C and eukaryotic prototype Nramp homologues, and among MntH C groups irrespective of bacterial phylogeny, indicate transfer toward bacteria of a eukaryotic prototype gene from an unidentified source.[70]

The three PmNramps appear as fairly close relatives of animal and higher-plant Nramp, like homologues found in most other

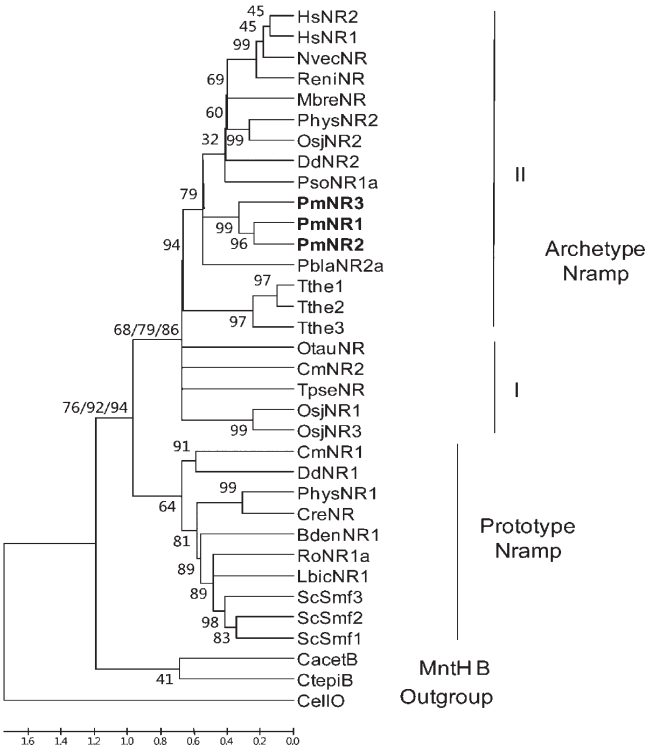

Figure 5. Simplified phylogeny of PmNramp1−3. The consensus tree presented was obtained using Mega 4.0;[38] it was linearized by assuming an equal evolutionary rate among lineages[84] and drawn to scale by calibration using a time of divergence between Nramp1 and -2 of 350 million years ago.[23] Phylogeny was inferred using a set of 340 parsimony-informative sites derived from full-length sequence initially aligned with the Muscle algorithm; the minimum evolution method was implemented on the basis of distances computed using the Equal Input a.a substitution model[85] and considering both differences in the composition bias among sequences and rate variation among sites modeled with a gamma distribution (shape parameter = 1.41). The percentages (>50%) of replicate tree nodes inferred from 3000 bootstrap samplings are indicated, while less reproducible partitions were collapsed. Percentage replicates of the main nodes (divergence of proto- and archetype Nramp; archetype I and II Nramp) obtained by other approaches are also indicated [maximum parsimony and maximum likelihood (Figure S2B,C of the Supporting Information)]. The nonlinearized version of this phylogenetic reconstruction is presented in Figure S6A of the Supporting Information, together with those produced by other approaches (Figure S6B,C of the Supporting Information) as well as using full-length sequences (Figure S6D,E of the Supporting Information). The following SLC11 phylogroups (bold) and full names of the organisms (italics) were included in this analysis: **Outgroup**, CellO, *Cellulophaga*; **MntH B**, CacetB, *Clostridium acetobutylicum*, CtepiB, *Chlorobium tepidum*; **Prototype Nramp**, ScSmf1−3, *S. cerevisiae*, LbicNR1, *Laccaria bicolor*, RoNR1a, *Rhizopus oryzae*, BdenNR1, *Batrachochytrium dendrobatidis*, CreNR, *Chlamydomonas reinhardtii*, PhysNR1, *Physcomitrella patens*, DdNR1, *Dictyostelium discoideum*, CmNR1, *Cyanidioschyzon merolae*; **Archetype Nramp, type I**, OsjNR1 and -3, *Oryza sativa japonica*, TpseNR, *Thalassiosira pseudoana*, CmNR2, *C. merolae*, OtauNR, *Ostreococcus tauri*; **Archetype Nramp, type II**, TtheNR1−3, *Tetrahymena thermophila*, PblaNR2, *Phycomyces blakesleeanus*, PmNR1−3, *P. marinus*, PsoNR1a, *Phytophthora sojae*, DdNR2, *D. discoideum*, OsjNR2, *O. sativa japonica*, PhysNR2, *Ph. patens*, MbreNR, *Monosiga brevicollis*, ReniNR, *Reniera*, NvecNR, *Nematostella vectensis*, HsNR1 and -2, *Homo sapiens*. The distribution of the taxa sampled is given in Table S2 of the Supporting Information.

chromoalveolate genomes to date, including some stramenopile species [e.g., PsoNR1a (Figure 5 and Table S4 of the Supporting Information)], and to a lesser extent those from apicomplexans and ciliates, which are more divergent [e.g., Tthe1−3 (Figure 3 and Figure S2 of the Supporting Information)]. Hence, the PmNramp sequences do not segregate with those of alveolatan relatives, as would be expected from the commonly accepted rRNA-based phylogeny that places dinoflagellates and apicomplexans as sister groups and ciliates diverging more basally;[71−73] this result may be a consequence of variations in DNA maintenance and overall GC percent, which is low in both ciliates and apicomplexans. Also, the extent of divergence among PmNramp polypeptides (e.g., PmNramp3) compared to other unicellular organisms that possess multiple *Nramp* genes indicated that PmNramps were more divergent than *T. thermophila* Nramps in various phylogenetic trees [longer branches for PmNramp homologues (Figure 3 and Figure S2 of the Supporting Information)] and resembled in this respect yeast Smfps, suggesting perhaps some biological significance.

Molecular Evolutionary Gene Analyses. To address the possibility that PmNramp3 diverged functionally, PmNramp sequence variations were examined further. With regard to the closely related *PmNramp1* and *PmNramp2* genes, the relative abundance of synonymous and nonsynonymous substitutions in codon-by-codon pairwise sequence comparisons showed purifying selection [$d_S - d_N = 5.45$ ($p = 0.000$) for pairwise deletion; $d_S - d_N = 6.056$ ($p = 0.000$) for complete deletion]. Tajima's test of the relative rate of exchange between aligned sequences supported the molecular clock hypothesis, i.e., similar evolutionary rates for *PmNramp1* and *PmNramp2* genes [χ^2 test values of 0.89 ($p = 0.346$) for nucleotide sequences and 0.11 ($p = 0.745$) for amino acid sequences]. Lastly, per site substitution patterns among aligned sequences were homogeneous, for both protein and nucleotide sequences [disparity indices of null and <0.260, respectively ($p > 0.1$)]. Thus, *PmNramp1* and *PmNramp2* gene sequences are homogeneous and evolve at similar rates under purifying selection that favors synonymous substitutions.

In contrast, comparison of the *PmNamp3* sequence with that of *PmNamp1* or *PmNamp2* showed a similar abundance of synonymous and nonsynonymous substitutions, indicating rather neutral evolution. Also, we detected unequal evolutionary rates between *PmNamp3* and *PmNamp1* or *PmNamp2* gene sequences [χ^2 test value of 57.56 ($p = 0.000$) or 71.87 ($p = 0.000$), respectively] and large numbers of unique transitions and transversions for the *PmNamp3* sequence (133 and 210, respectively) relativel to *PmNramp1* (86 and 85, respectively) or *PmNramp2* (77 and 77, respectively). PmNramp3 protein had a distinct rate of evolution compared to PmNramp1 or -2 [χ^2 test value of 30.83 ($p = 0.000$) or 27.61 ($p = 0.000$), respectively], and we measured the heterogeneous pattern of substitution per site by comparing PmNramp3 and PmNramp2 protein sequences [disparity index of 0.449 ($p = 0.019$)].

To demonstrate that *PmNramp* gene diversity reflects accelerated evolution in areas of the molecule otherwise nonconserved, we conducted detection of regions under evolutionary selection (Figure S3 of the Supporting Information) using a sliding window to calculate dN/dS variations and a Java Codon Delimited Alignment and Phylogenetic Analysis using Maximum Likelihood (JCoDA and PAML).[41,42] As expected, little evidence of potential positive selection was obtained, and superposing the results of sliding window analysis and predicted transmembrane topology showed they were mostly confined to nonmembranous parts of PmNramps (Figure S3 of the Supporting Information). Site-specific likelihood ratio test (LRT) analyses further confirmed

discrete classes of sites along the aligned PmNramps but failed to detect evidence of positive selection (in both M1a vs M2a and M7 vs M8 models),[41,42] thus indicating that *PmNramp* genes are essentially subjected to strong purifying selection.

Thus, the significant divergence among PmNramp parologs was not related to the diversification of critical functional elements, which remained constrained by purifying selection, but seems to rather affect extramembranous determinants of protein expression, localization, and trafficking. Our results suggest that *PmNramp* genes evolved by successive duplications of *PmNramp2*, first yielding *PmNramp3* and more recently *PmNramp1*. This interpretation is further supported by the fact that *PmNramp1* and *PmNramp2* are highly similar in terms of exon−intron splicing site distribution, while *PmNramp3* displays a distinct pattern of splice site distribution as shown by arrows in Figure 3.

Functional Analysis of PmNramp Isotypes by Yeast Complementation. To test whether PmNramp isotypes transport Fe^{2+}, cDNAs of the three *PmNramp* homologues tagged with an HA epitope were cloned in expression vector pFL61 and used to transform iron transport mutant yeast strain DEY1453 (*fet3fet4*). This mutant grows poorly on media with low iron concentrations because the high-affinity (*fet3*) and low-affinity (*fet4*) Fe^{2+} transporters have been disrupted.[46] Prior to the complementation assay, *PmNramp1* was confirmed to be both transcribed and translated in the transformed yeast (Figure 6A). Yeast expressing PmNramp1 grew better than yeast containing the empty cloning vector on media either lacking or supplemented with 2 μM $FeCl_3$ (Figure 6B). The growth curves of yeast transformed with PmNramp1 entered the exponential growth phase much earlier than cells transformed with the pFL61 vector alone (Figure 6C), thereby demonstrating the function of PmNramp1 as a divalent cation transporter in the uptake of exogenous iron. Although we have previously shown that iron is important for the growth and survival of *P. marinus*,[8,9] this is the first functional characterization of an iron uptake pathway in this parasite.

Neither PmNramp3 nor PmNramp2 complemented the mutant yeast under conditions suitable for PmNramp1 activity. PmNramp2 was not transcribed in the transformed yeast (Figure S4A of the Supporting Information), thereby providing a rationale for the lack of complementation of the mutant. In contrast, the PmNramp3 protein was expressed in the transformed yeast, although at a level lower than that of PmNramp1 (Figure S4A of the Supporting Information). Thus, the lack of iron uptake in the mutant yeast transformed with PmNramp3 (Figure S4B,C of the Supporting Information) could be due to lower level of expression or localization in subcellular compartments other than the plasma membrane. Because the N- and C-termini are the most divergent parts of PmNramp (Figure 3 and Figure S3 of the Supporting Information) and because swapping of the N- and C-termini of Nramp2 with Smf1p improved heterologues of the yeast protein in *Xenopus* oocytes,[74,75] we applied a similar strategy by inserting PmNramp2 and -3 hydrophobic core between the N- and C-termini of PmNramp1 (Figure S5 of the Supporting Information). Immunofluorescence staining of yeast cells transformed with chimeric PmNramp3 showed peripheral localizations (Figure 7A). The resulting chimeric PmNramp3 showed significant complementation activity in both solid and liquid medium (Figure 7B,C), while chimeric PmNramp2, like its native counterpart, was still not expressed in the transformed yeast mutant (data not shown). In this regard, we noted that the PmNramp2 sequence diverged specifically in a few areas of the hydrophobic core [e.g., PmNramp2-specific sequence underlined (see Figure 3 and Figure S3 of the Supporting Information), RVSNI in TMS3, MRVM in TMS5, ELVGI in TMS6, and EFVKQ in TMS7, also FALNR in TMS11], which might contribute to the impairment of PmNramp2 heterologous expression. Nevertheless, the fact that both PmNramp1 and PmNramp3 can function as iron transporters is consistent with the selective preservation of critical TM functional elements among PmNramp parologs as revealed by our molecular evolution analyses.

To examine the specificity of PmNramp1 in cation transport, we tested its ability to complement the yeast mutant *smf1smf2* that has less ability to acquire manganese and cannot grow in the presence of low EGTA concentrations. No significant growth was detected in minimal medium with 1.5 and 2.25 mM EGTA. Addition of manganese to the EGTA-containing medium failed to promote growth of mutant yeast transformed with the PmNramp isotypes, in contrast with the Smf1p-complemented yeast (Figure S7A of the Supporting Information). Another phenotype of the *smf1smf2* mutant is poor growth under alkaline conditions due to the lack of manganese acquisition. While the mutant transformed with the PmNramp isotypes did not show any improved growth at pH 7.9, Smf1 could rescue yeast growth under the same conditions (Figure S7B of the Supporting Information). The results show that PmNramp1 did not transport manganese under the conditions tested. Although manganese is required for the activity of many enzymes, including certain sugar transferases,[76] and is a cofactor for SOD in some organisms,[77] it does not display the functional versatility of iron. Some Nramp homologues, including mouse Nramp1 and Nramp2, as well as plant Nramp homologues are effective in transporting both iron and manganese, while *S. cerevisiae* Nramp homologues Smf1 and Smf2 may prefer manganese over iron.[24,78−80] Given their phylogenetic position, it seems possible that PmNramp1 and -3 can transport Mn and using the yeast *smf1 sod1* double mutant strain that requires Mn to survive[55] could facilitate the detection of PmNramp-dependent Mn import. Additional studies optimizing the heterologous expression level and intracellular targeting or using more quantitative approaches will be required to determine whether PmNramp1 cation transport specificity is restricted relative to the examples described above or include Mn as well. It is noteworthy that a search of potential manganese transporters in the *P. marinus* genome revealed a potential homologue of the yeast low-affinity manganese transporter PHO84, suggesting an alternative mechanism for manganese uptake in *Perkinsus*.

Site-Directed Mutagenesis of PmNramp1 Predicted Functional Residues. A multiple-structure superposition of the X-ray structures of five cation-driven transporters with inverted symmetry was obtained, allowing flexibilities to take into account the distinct geometries that correspond to different conformations in the conserved transport cycle: two open to out, one occluded from both sides, and two open to in (Mhp1, LeuT, BetP, SGLT1, and ApcT, respectively). Though these structures represent distant families of transporters, superposition demonstrates remarkable spatial conservation: a common core spanning ~200 equivalent positions (e.p.) and a 3.4 Å overall root-mean-square deviation (rmsd). The rmsd is not distributed homogeneously along the 10-TMS hydrophobic core; for instance, TMS1 exhibits remarkable 3D conservation, while the structure of TMS6 apparently evolved with fewer constraints (Figure 8A, left panel). It seems there is a functional correlate as LeuT (Slc6) TMS1

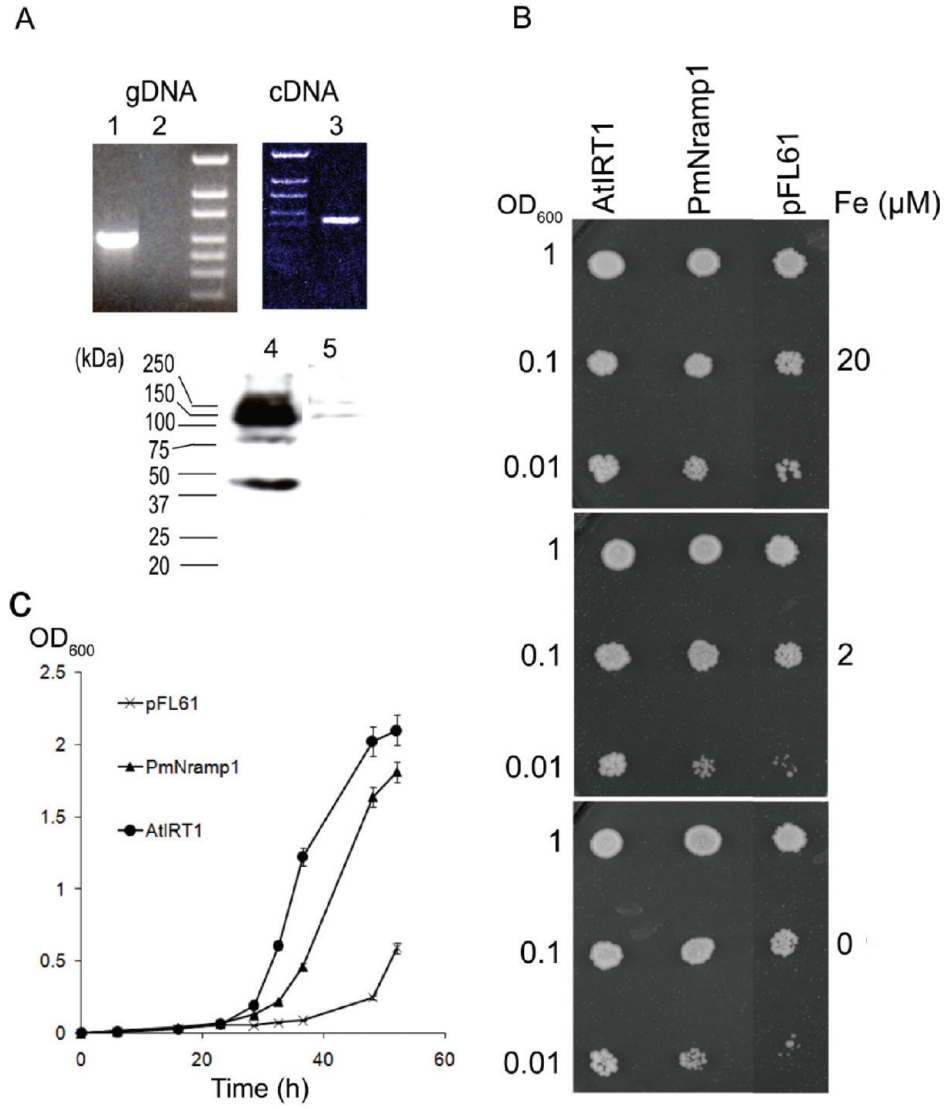

Figure 6. *PmNramp1* complements yeast *fet3fet4* iron deficiency. *S. cerevisiae* strain *fet3fet4* was transformed with the pFL61 expression plasmid along with pFL61 containing full-length cDNA for PmNramp1 tagged with the HA epitope or positive control *AtIRT1*. (A) Expression of PmNramp1 in yeast. Genomic DNA (gDNA) extracted from yeast transformed with *PmNramp1* (lane 1) or pFL61 (lane 2) was used as a template in PCR to confirm the presence of the *PmNramp1*-containing vector in yeast cells; RT-PCR was performed to check the expression of *PmNramp1* mRNA in yeast (lane 3). Enriched membrane fractions were prepared from yeast transformed with PmNramp1 (lane 4) or pFL61 (lane 5), separated by 12% sodium dodecyl sulfate−polyacrylamide gel electrophoresis, and analyzed by immunoblotting with the anti-HA high-affinity 3F10 antibody conjugated with biotin and strepatavidin conjugated with horseradish peroxidase. The positions of reference molecular mass markers are indicated to the left of the immunoblot. (B and C) Functional analysis of PmNramp1 activity in yeast cells. (B) Growth of *PmNramp1*, *AtIRT1*, and negative control (pFL61) transformed *fet3fet4* serially diluted cells after 5 days at 30 °C on SD medium supplemented with 50, 20, or 0 μM $FeCl_3$. (C) Growth in liquid SD medium supplemented with 20 μM $FeCl_3$.

interacts with both the driving cation (dark blue sticks) and substrate (orange sticks), and TMS6 binds only the substrate (orange sticks). One speculation is that TMS6 evolved in relation to different substrate geometries and TMS1 coupled the cation-driving force and substrate translocation pathway. The triplets targeted for mutagenesis represent candidate substrate binding contacts on both TMS1 (DPG, Mut1 and -2) and TMS6 (MPH, Mut3 and -4).

Mutation of the targeted amino acids in TMS1 and TMS6 abrogated PmNramp1 iron uptake activity in yeast mutant *fet3fet4*. The loss of complementation resulted from both single and double mutations on each of the TMS (Figure 8C,D). Inspection of protein expression levels of the mutants tested showed that mutations in TMS1 significantly reduced the level of PmNramp1 expression in yeast, while mutations in TMS6 preserved PmNramp1 heterologous expression levels (Figure 8A, right panel). Although the equivalent TMS1 mutants in the *E. coli* MntH or mouse Nramp2 are efficiently expressed in the homologous cells and demonstrate impaired transport activity, when introduced in yeast, the mouse Nramp2 D86A mutant exhibits a drastically reduced level of expression.[81] This suggests that mutations in TMS1 may have more impact on Nramp expression in heterologous expression systems than in the homologous cells. The use of knockdown approaches[82] together with the transformation methodology we recently developed[15] should allow further detailed functional studies in the homologous *Perkinsus* cells to

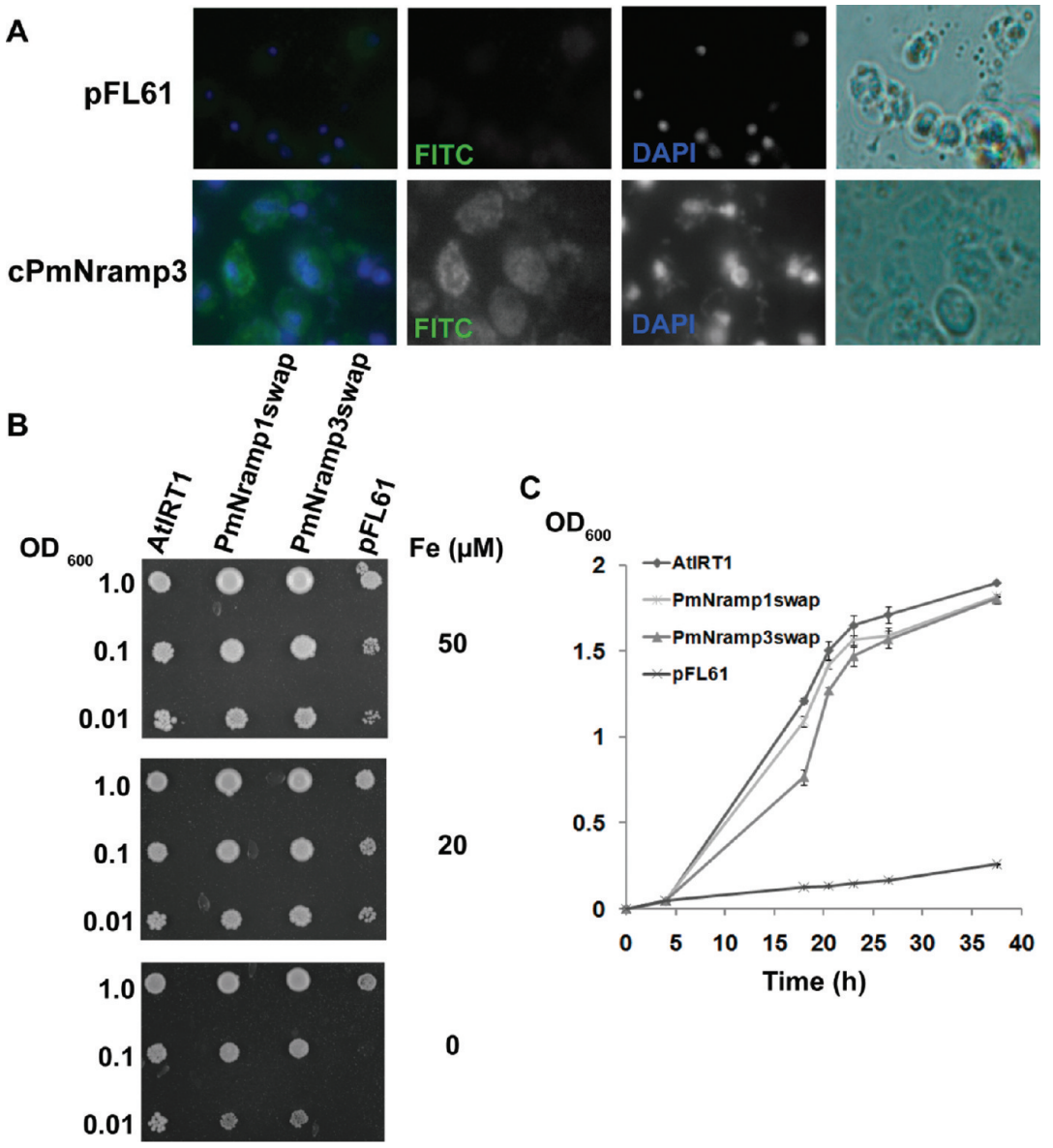

Figure 7. Complementation of the yeast *fet3fet4* iron deficiency phenotype by PmNramp3 after swapping of N- and C-termini. (A) Immunofluorescence staining of yeast cells transformed with chimeric PmNramp3. PmNramp3 protein was detected by mouse anti-HA monoclonal antibody and anti-mouse IgG conjugated with fluorescein isothiocyanate. The positions of nuclei were revealed by DAPI staining. (B) Growth of serially diluted cells transformed with PmNramp1 and PmNramp3 after domain swapping (PmNramp1swap and PmNramp3swap, respectively) after 5 days at 30 °C on SD medium supplemented with 50, 20, or 0 μM $FeCl_3$. (C) Growth in liquid SD medium supplemented with 20 μM $FeCl_3$.

determine rigorously whether mutations in TMS1 can impair metal transport without affecting protein expression. PmNramp1 mutants with mutations in TMS6 were expressed at levels similar to that of wild-type PmNramp1 (Figure 8A, top right panel), and immunofluorescence staining revealed no change in localization of the mutant PmNramp1 in yeast cells (Figure 8B).

The results from our functional studies buttress the relevance of the TMS 1 and -6 predicted to exert pseudosymmetric roles in substrate transport. The exquisite sensitivity of TMS1 to mutagenesis is demonstrated by a reduced level of protein expression and the loss of transport activity after mutations considered biochemically conservative (Asp76Glu and Gly78Ala), and the results support a possible direct role of TMS6 residues in substrate binding, notably the Slc11-specific TMS6 His that is required for divalent metal uptake. Experimental data are also in line with our observations that Slc11 TMS6 triplet MPH changed repeatedly during evolution, from the outgroup to the Slc11 family and from Slc11 archetype I to the Nrat1 variant (ref 61 and Figure S1 of the Supporting Information). Together, our results fit a pseudosymmetric 3D model for Slc11 with critical structural constraints exerted on TMS1 and TMS6 substrate binding activity. These results provide novel functional evidence supporting the LeuT 3D model for the Slc11 family that is based on remote homology with cation-driven transporters with inverted symmetry.

The functional data reinforce the proposed PmNramp1 homologous structural model and, together with the molecular evolutionary gene analyses indicating that the hydrophobic core

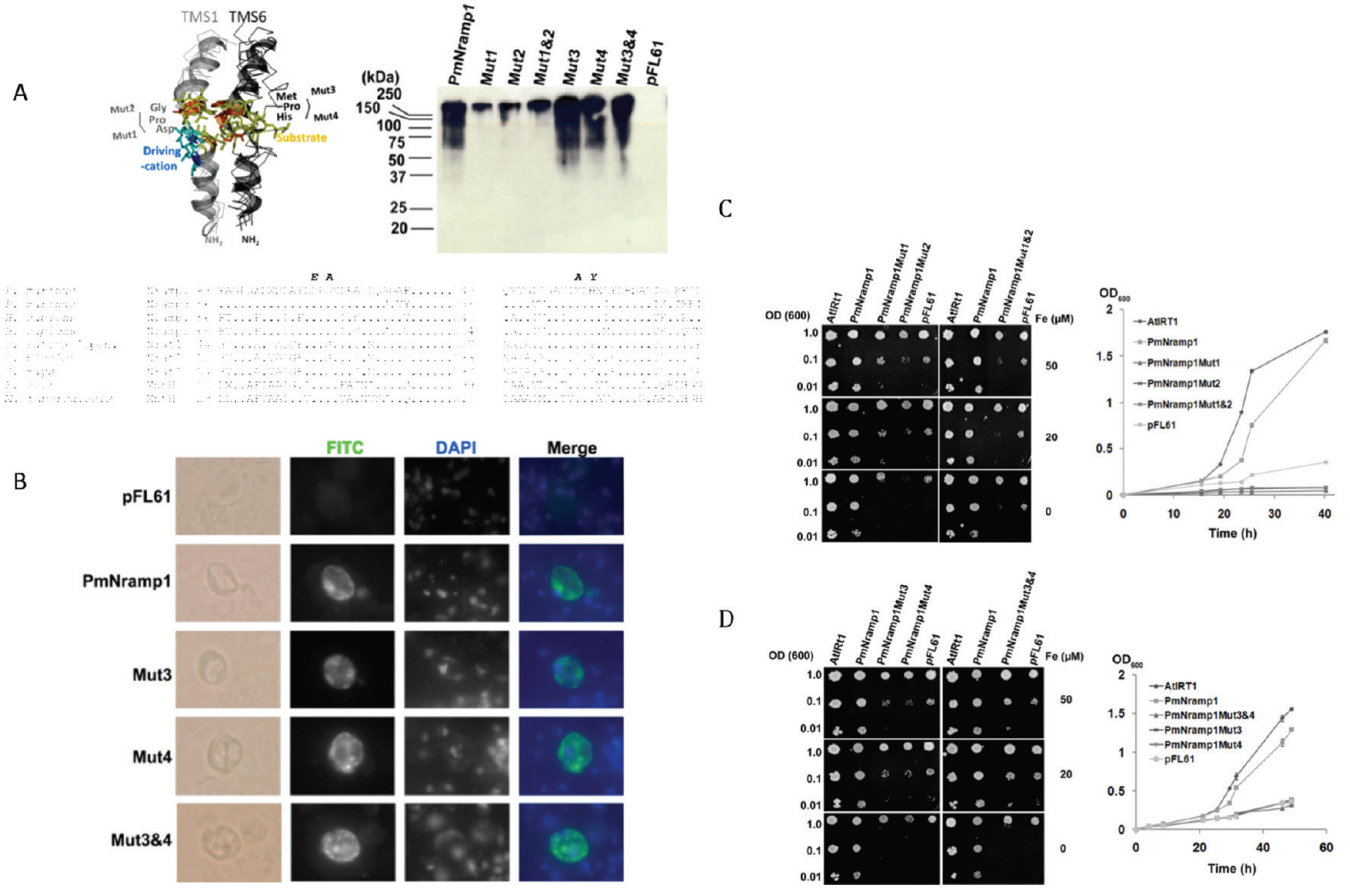

Figure 8. PmNramp1 TMS6 predicted key residues are required for Fe^{2+} uptake. (A) The top left panel shows a view of superimposed TMS1 and TMS6 of carriers from five evolutionarily distant families (Mhp1/NCS1, LeuT/NSS/Slc6, BetP/BCCT, vSGLT1/SSS/Slc5, and ApcT/APC/Slc7) showing LeuT residues engaged in substrate binding (orange sticks) and those interacting with the driving cation (Na2 site, dark blue sticks); the corresponding sites in other transporters are represented with yellow and light blue sticks, respectively. The areas targeted for mutagenesis are indicated. The top right panel shows a Western blot of the membrane-enriched extract from yeast cells transformed with mutated PmNramp1. The bottom panel shows MSA corresponding to TMS1 and TMS6 showing natural variation among Nramp/MntH family members and Nrat1 variants as well as the positions of the sites, which were targeted for PmNramp1 mutagenesis. (B) Immunofluorescence staining of yeast cells transformed with PmNramp1TMS6 mutants. PmNramp1 protein was detected with the mouse anti-HA monoclonal antibody and anti-mouse IgG conjugated with IFTC. The positions of nuclei were revealed by DAPI staining. (C) Growth of serially diluted cells transformed with PmNramp1 with mutations at TMS1 after 5 days at 30 °C on SD medium supplemented with 50, 20, or 0 μM $FeCl_3$ (left). Growth of TMS1 mutants in liquid SD medium supplemented with 20 μM $FeCl_3$ (right). (D) Growth of serially diluted cells transformed with PmNramp1 with mutations at TMS6 after 5 days at 30 °C on SD medium supplemented with 50, 20, or 0 μM $FeCl_3$ (left). Growth of TMS6 mutants in liquid medium supplemented with 20 μM $FeCl_3$ (Mut1, Asp76Glu; Mut2, Gly78Ala; Mut1&2, Asp76Glu/Gly78Ala; Mut3, Met250Ala; Mut 4, His252Tyr; Mut3&4, Met250Ala/His252Tyr) (right).

of PmNramp paralogs remained constrained by purifying selection, suggest that PmNramps function as proton-dependent transporters of divalent iron. Although PmNramp1 failed to transport manganese under the conditions tested, because most Slc11 homologues exhibit relatively low selectivity for divalent metals, it is possible that PmNramps can transport other metals. Constitutive mRNA expression of *PmNramp1*−*3* in trophozoites in vitro and extensive protein sequence variation in extramembranous regions raise the possibility of dynamic post-translational control of expression, location, and turnover of PmNramps. One possible scenario is that PmNramp1 might function as the prominent isotype for uptake of exogenous iron into the parasite cells, whereas PmNramp2 and PmNramp3 could function downstream of PmNramp1 for intracellular iron trafficking in relocation and storage. The key finding that PmNramp1 functions in uptake of exogenous iron provides the molecular and biochemical basis for prior observations of the effect of environmental iron in enhancing infection prevalence and intensity, promoting parasite proliferation, and upregulating expression of virulence factors such as PmSOD1. The identification of PmNramp1 as a possible mediator of parasite virulence opens new avenues for exploring novel strategies of intervention. Further, because of the basal phylogenetic position of *P. marinus* within the Alveolata,[31] the structural and functional characterization of the multiple PmNramp isotypes will significantly contribute to an improved understanding of metal acquisition mechanisms in intracellular protozoan parasites.

■ ASSOCIATED CONTENT

Supporting Information. Additional phylogenetic analyses, sequence alignments, and a list of primers. This material is available free of charge via the Internet at http://pubs.acs.org.

AUTHOR INFORMATION

Corresponding Author

*Department of Microbiology and Immunology, University of Maryland School of Medicine, IMET, 701 E. Pratt St., Suite 236, Baltimore, MD 21202-3101. Phone: (410) 234-8826. Fax: (410) 234-8896. E-mail: gvasta@som.umaryland.edu.

ACKNOWLEDGMENT

We thank Dr. Malcolm K. Jones (Queensland Institute of Medical Research, Brisbane, Australia) and Dr. David Eide (University of Wisconsin, Madison, WI) for providing the yeast strains. This work was supported by grants IOS 0958016 and IOS 0321417 from the National Science Foundation and grants NA05OAR4171042/SA7528082-O and SA7528068-I from Maryland Sea Grant, NOAA, U.S. DOC to G.R.V, and in part by grant NSF/USDA 0333240 from the NSF/USDA-CSREES Microbial Sequencing Program to G.R.V and J.A.F.R.

ABBREVIATIONS

DMT1, divalent metal transporter 1; IRE, iron responsive element; IRP, iron responsive element binding protein; MntH, proton-dependent manganese transport; Nramp, natural resistance-associated macrophage protein; RACE, rapid amplification of cDNA ends; RT-PCR, reverse transcription polymerase chain reaction; Slc, solute carrier; TMS, transmembrane segment; UTR, untranslated region.

REFERENCES

(1) Harvell, C. D., Kim, K., Burkholder, J. M., Colwell, R. R., Epstein, P. R., Grimes, D. J., Hofmann, E. E., Lipp, E. K., Osterhaus, A. D., Overstreet, R. M., Porter, J. W., Smith, G. W., and Vasta, G. R. (1999) Emerging marine diseases: Climate links and anthropogenic factors. *Science 285*, 1505–1510.

(2) Tasumi, S., and Vasta, G. R. (2007) A galectin of unique domain organization from hemocytes of the Eastern oyster (*Crassostrea virginica*) is a receptor for the protistan parasite *Perkinsus marinus*. *J. Immunol. 179*, 3086–3098.

(3) Perkins, F. O. (1996) The structure of *Perkinsus marinus* (Mackin, Owen and Collier, 1950) Levine, 1978 with comments on taxonomy and phylogeny of *Perkinsus* spp. *J. Shellfish Res. 15*, 67–87.

(4) Ford, S. E., and Chintala, M. M. (2006) Northward expansion of a marine parasite: Testing the role of temperature adaptation. *J. Exp. Mar. Biol. Ecol. 339*, 226–235.

(5) Pecher, W. T., Alavi, M. R., Schott, E. J., Fernández-Robledo, J. A., Roth, L., Berg, S. T., and Vasta, G. R. (2008) Assessment of the northern distribution range of selected *Perkinsus* species in eastern oysters (*Crassostrea virginica*) and hard clams (*Mercenaria mercenaria*) with the use of PCR-based detection assays. *J. Parasitol. 94*, 410–422.

(6) Doherty, C. P. (2007) Host-pathogen interactions: The role of iron. *J. Nutr. 137*, 1341–1344.

(7) Volety, A. K. (2008) Effects of salinity, heavy metals and pesticides on health and physiology of oysters in the Caloosahatchee Estuary, Florida. *Ecotoxicology 17*, 579–590.

(8) Lin, Z., Fernández-Robledo, J.-A., Cellier, M. F. M., and Vasta, G. R. (2009) Metals and membrane metal transporters in biological systems: The role(s) of Nramp in host-parasite interactions. *J. Argent. Chem. Soc. 97*, 210–225.

(9) Gauthier, J. D., and Vasta, G. R. (1994) Inhibition of in vitro replication of the oyster parasite *Perkinsus marinus* by the natural iron chelators transferrin, lactoferrin, and desferrioxamine. *Dev. Comp. Immunol. 18*, 277–286.

(10) Schott, E. J., Pecher, W. T., Okafor, F., and Vasta, G. R. (2003) The protistan parasite *Perkinsus marinus* is resistant to selected reactive oxygen species. *Exp. Parasitol. 105*, 232–240.

(11) Anderson, R. S. (1999) Lack of hemocyte chemiluminescence stimulation by *Perkinsus marinus* in eastern oysters *Crassostrea virginica* with Dermo diseases. *J. Aquat. Anim. Health 11*, 179–182.

(12) Volety, A. K., and Chu, F. L. (1995) Suppression of chemiluminescence of eastern oyster (*Crassostrea virginica*) hemocytes by the protozoan parasite *Perkinsus marinus*. *Dev. Comp. Immunol. 19*, 135–142.

(13) Alavi, M. R., Fernández-Robledo, J. A., and Vasta, G. R. (2009) In vitro intracellular survival of *Perkinsus marinus* trophozoites upon phagocytosis by oyster (*Crassostrea virginica* and *Crassostrea ariakensis*) hemocytes. *J. Parasitol. 95*, 900–907.

(14) Asojo, O. A., Schott, E. J., Vasta, G. R., and Silva, A. M. (2006) Structures of PmSOD1 and PmSOD2, two superoxide dismutases from the protozoan parasite *Perkinsus marinus*. *Acta Crystallogr. F62*, 1072–1075.

(15) Fernández-Robledo, J. A., Lin, Z., and Vasta, G. R. (2008) Transfection of the protozoan parasite *Perkinsus marinus*. *Mol. Biochem. Parasitol. 157*, 44–53.

(16) Schott, E. J., Robledo, J. A. F., Wright, A. C., Silva, A. M., and Vasta, G. R. (2003) Gene organization and homology modeling of two iron superoxide dismutases of the early branching protist *Perkinsus marinus*. *Gene 309*, 1–9.

(17) Schott, E. J., and Vasta, G. R. (2003) The PmSOD1 gene of the protistan parasite *Perkinsus marinus* complements the *sod2*Δ mutant of *Saccharomyces cerevisiae*, and directs an iron superoxide dismutase to mitochondria. *Mol. Biochem. Parasitol. 126*, 81–92.

(18) Wright, A. C., Ahmed, H., Gauthier, J. D., Silva, A. M., and Vasta, G. R. (2002) cDNA cloning and characterization of two iron superoxide dismutases from the oyster parasite *Perkinsus marinus*. *Mol. Biochem. Parasitol. 123*, 73–77.

(19) Gauthier, J. D. (1998) Development and utilization of an in vitro culture system for the characterization of gene expression in the oyster parasite *Perkinsus marinus*. Ph.D. Dissertation, University of Maryland, College Park, MD.

(20) Flannagan, R. S., Cosio, G., and Grinstein, S. (2009) Antimicrobial mechanisms of phagocytes and bacterial evasion strategies. *Nat. Rev. Microbiol. 7*, 355–366.

(21) Cellier, M., Prive, G., Belouchi, A., Kwan, T., Rodrigues, V., Chia, W., and Gros, P. (1995) Nramp defines a family of membrane proteins. *Proc. Natl. Acad. Sci. U.S.A. 92*, 10089–10093.

(22) Cohen, A., Nelson, H., and Nelson, N. (2004) *The Nramp family*, Kluwer Academic/Landes, New York.

(23) Cellier, M. F., Courville, P., and Campion, C. (2007) Nramp1 phagocyte intracellular metal withdrawal defense. *Microbes Infect. 9*, 1662–1670.

(24) Jabado, N., Lam-Yuk-Tseung, S., Forbes, J. R., and Gros, P. (2004) *Mouse Nramp1 resistance associated macrophage protein 1 (Nramp1): A key player in host innate immunity against infections*, Landes Bioscience/Kluwer Academic, New York.

(25) Landfear, S. M. (2011) Nutrient transport and pathogenesis in selected parasitic protozoa. *Eukaryotic Cell*.

(26) Boyer, E., Bergevin, I., Malo, D., Gros, P., and Cellier, M. F. (2002) Acquisition of Mn(II) in addition to Fe(II) is required for full virulence of *Salmonella enterica* serovar Typhimurium. *Infect. Immun. 70*, 6032–6042.

(27) Domenech, P., Pym, A. S., Cellier, M., Barry, C. E., III, and Cole, S. T. (2002) Inactivation of the *Mycobacterium tuberculosis* Nramp orthologue (mntH) does not affect virulence in a mouse model of tuberculosis. *FEMS Microbiol. Lett. 207*, 81–86.

(28) Boechat, N., Lagier-Roger, B., Petit, S., Bordat, Y., Rauzier, J., Hance, A. J., Gicquel, B., and Reyrat, J. M. (2002) Disruption of the gene homologous to mammalian Nramp1 in *Mycobacterium tuberculosis* does not affect virulence in mice. *Infect. Immun. 70*, 4124–4131.

(29) Anderson, E. S., Paulley, J. T., Gaines, J. M., Valderas, M. W., Martin, D. W., Menscher, E., Brown, T. D., Burns, C. S., and Roop, R. M., II (2009) The manganese transporter MntH is a critical virulence

determinant for *Brucella abortus* 2308 in experimentally infected mice. *Infect. Immun. 77*, 3466–3474.

(30) Fernández-Robledo, J. A., Courville, P., Cellier, M. F., and Vasta, G. R. (2004) Gene organization and expression of the divalent cation transporter Nramp in the protistan parasite *Perkinsus marinus*. *J. Parasitol. 90*, 1004–1014.

(31) Saldarriaga, J. F., McEwan, M. L., Fast, N. M., Taylor, F. J. R., and Keeling, P. J. (2003) Multiple protein phylogenies show that *Oxyrrhis marina* and *Perkinsus marinus* are early branches of the dinoflagellate lineage. *Int. J. Syst. Evol. Microbiol. 53*, 355–365.

(32) Gauthier, J. D., and Vasta, G. R. (1995) In vitro culture of the eastern oyster parasite *Perkinsus marinus*: Optimization of the methodology. *J. Invertebr. Pathol. 66*, 156–168.

(33) Borson, N. D., Salo, W. L., and Drewes, L. R. (1992) A lock-docking oligo(dT) primer for 5′ and 3′ RACE PCR. *PCR Methods Appl. 2*, 144–148.

(34) Courville, P., Urbankova, E., Rensing, C., Chaloupka, R., Quick, M., and Cellier, M. F. (2008) Solute carrier 11 cation symport requires distinct residues in transmembrane helices 1 and 6. *J. Biol. Chem. 283*, 9651–9658.

(35) Czachorowski, M., Lam-Yuk-Tseung, S., Cellier, M., and Gros, P. (2009) Transmembrane topology of the mammalian Slc11a2 iron transporter. *Biochemistry 48*, 8422–8434.

(36) Roy, A., Kucukural, A., and Zhang, Y. (2010) I-TASSER: A unified platform for automated protein structure and function prediction. *Nat. Protoc. 5*, 725–738.

(37) Thomson, J. D., Gibson, T. J., and Higgins, D. G. (2002) *Current Protocols in Bioinformatics*, Chapter 2, Unit 2.3, Wiley, New York.

(38) Tamura, K., Dudley, J., Nei, M., and Kumar, S. (2007) MEGA4: Molecular Evolutionary Genetics Analysis (MEGA) software version 4.0. *Mol. Biol. Evol. 24*, 1596–1599.

(39) Whelan, S., and Goldman, N. (2001) A general empirical model of protein evolution derived from multiple protein families using a maximum-likelihood approach. *Mol. Biol. Evol. 18*, 691–699.

(40) Schmidt, H. A., and von Haeseler, A. (2007) Maximum-likelihood analysis using TREE-PUZZLE. *Current Protocols in Bioinformatics*, Chapter 6, Unit 6.6, Wiley, New York.

(41) Steinway, S. N., Dannenfelser, R., Laucius, C. D., Hayes, J. E., and Nayak, S. (2010) JCoDA: A tool for detecting evolutionary selection. *BMC Bioinf. 11*, 284.

(42) Yang, Z. (2007) PAML 4: Phylogenetic analysis by maximum likelihood. *Mol. Biol. Evol. 24*, 1586–1591.

(43) Goodstadt, L., and Ponting, C. P. (2005) Mammalian Genes and Evolutionary Genomics. In *The Proteomics Protocols Handbook* (Walker, J. M., Ed.) pp 543−553, Humana Press Inc., Totowa, NJ.

(44) Eide, D., Broderius, M., Fett, J., and Guerinot, M. L. (1996) A novel iron-regulated metal transporter from plants identified by functional expression in yeast. *Proc. Natl. Acad. Sci. U.S.A. 93*, 5624–5628.

(45) Kaiser, B. N., Moreau, S., Castelli, J., Thomson, R., Lambert, A., Bogliolo, S., Puppo, A., and Day, D. A. (2003) The soybean NRAMP homologue, GmDMT1, is a symbiotic divalent metal transporter capable of ferrous iron transport. *Plant J. 35*, 295–304.

(46) Eide, D., Davis-Kaplan, S., Jordan, I., Sipe, D., and Kaplan, J. (1992) Regulation of iron uptake in *Saccharomyces cerevisiae*. The ferrireductase and Fe(II) transporter are regulated independently. *J. Biol. Chem. 267*, 20774–20781.

(47) Vert, G., Grotz, N., Dedaldechamp, F., Gaymard, F., Guerinot, M. L., Briat, J. F., and Curie, C. (2002) IRT1, an *Arabidopsis* transporter essential for iron uptake from the soil and for plant growth. *Plant Cell 14*, 1223–1233.

(48) Zhang, H., Dungan, C. F., and Lin, S. (2011) Introns, alternative splicing, spliced leader trans-splicing and differential expression of pcna and cyclin in *Perkinsus marinus*. *Protist 162*, 154–167.

(49) Mayer, M. G., and Floeter-Winter, L. M. (2005) Pre-mRNA trans-splicing: From kinetoplastids to mammals, an easy language for life diversity. *Mem. Inst. Oswaldo Cruz 100*, 501–513.

(50) Laird, P. W. (1989) Trans splicing in trypanosomes: Archaism or adaptation? *Trends Genet. 5*, 204–208.

(51) Wang, Z., Morris, J. C., Drew, M. E., and Englund, P. T. (2000) Inhibition of *Trypanosoma brucei* gene expression by RNA interference using an integratable vector with opposing T7 promoters. *J. Biol. Chem. 275*, 40174–40179.

(52) Portnoy, M. E., Jensen, L. T., and Culotta, V. C. (2002) The distinct methods by which manganese and iron regulate the Nramp transporters in yeast. *Biochem. J. 362*, 119–124.

(53) Liu, X. F., Elashvili, I., Gralla, E. B., Valentine, J. S., Lapinskas, P., and Culotta, V. C. (1992) Yeast lacking superoxide dismutase. Isolation of genetic suppressors. *J. Biol. Chem. 267*, 18298–18302.

(54) Foot, N. J., Leong, Y. A., Dorstyn, L. E., Dalton, H. E., Ho, K., Zhao, L., Garrick, M. D., Yang, B., Hiwase, D., and Kumar, S. (2011) Ndfip1-deficient mice have impaired DMT1 regulation and iron homeostasis. *Blood 117*, 638–646.

(55) Reddi, A. R., Jensen, L. T., and Culotta, V. C. (2009) Manganese homeostasis in *Saccharomyces cerevisiae*. *Chem. Rev. 109*, 4722–4732.

(56) Forrest, L. R., Kramer, R., and Ziegler, C. (2011) The structural basis of secondary active transport mechanisms. *Biochim. Biophys. Acta 1807*, 167–188.

(57) Weyand, S., Shimamura, T., Beckstein, O., Sansom, M. S., Iwata, S., Henderson, P. J., and Cameron, A. D. (2011) The alternating access mechanism of transport as observed in the sodium-hydantoin transporter Mhp1. *J. Synchrotron Radiat. 18*, 20–23.

(58) Krishnamurthy, H., Piscitelli, C. L., and Gouaux, E. (2009) Unlocking the molecular secrets of sodium-coupled transporters. *Nature 459*, 347–355.

(59) Abramson, J., and Wright, E. M. (2009) Structure and function of Na^+-symporters with inverted repeats. *Curr. Opin. Struct. Biol. 19*, 425–432.

(60) Khafizov, K., Staritzbichler, R., Stamm, M., and Forrest, L. R. (2010) A study of the evolution of inverted-topology repeats from LeuT-fold transporters using AlignMe. *Biochemistry 49*, 10702–10713.

(61) Cellier, M. (2011) Nutritional Immunity: Homology Modeling of Nramp Metal Import. In *Current Topics in Innate Immunity* (Lambris, J. D., Ed.) Vol. II, pp 1−14, Wiley, New York.

(62) Chaloupka, R., Courville, P., Veyrier, F., Knudsen, B., Tompkins, T. A., and Cellier, M. F. (2005) Identification of functional amino acids in the Nramp family by a combination of evolutionary analysis and biophysical studies of metal and proton cotransport in vivo. *Biochemistry 44*, 726–733.

(63) Xia, J., Yamaji, N., Kasai, T., and Ma, J. F. (2010) Plasma membrane-localized transporter for aluminum in rice. *Proc. Natl. Acad. Sci. U.S.A. 107*, 18381–18385.

(64) Knudsen, B., and Miyamoto, M. M. (2003) Sequence alignments and pair hidden Markov models using evolutionary history. *J. Mol. Biol. 333*, 453–460.

(65) Cellier, M., Belouchi, A., and Gros, P. (1996) Resistance to intracellular infections: Comparative genomic analysis of Nramp. *Trends Genet. 12*, 201–204.

(66) Ben-Yona, A., and Kanner, B. I. (2009) Transmembrane domain 8 of the γ-aminobutyric acid transporter GAT-1 lines a cytoplasmic accessibility pathway into its binding pocket. *J. Biol. Chem. 284*, 9727–9732.

(67) Kaufmann, K. W., Dawson, E. S., Henry, L. K., Field, J. R., Blakely, R. D., and Meiler, J. (2009) Structural determinants of species-selective substrate recognition in human and *Drosophila* serotonin transporters revealed through computational docking studies. *Proteins 74*, 630–642.

(68) Nikko, E., Sullivan, J. A., and Pelham, H. R. (2008) Arrestin-like proteins mediate ubiquitination and endocytosis of the yeast metal transporter Smf1. *EMBO Rep. 9*, 1216–1221.

(69) Jensen, L. T., Carroll, M. C., Hall, M. D., Harvey, C. J., Beese, S. E., and Culotta, V. C. (2009) Down-regulation of a manganese transporter in the face of metal toxicity. *Mol. Biol. Cell 20*, 2810–2819.

(70) Richer, E., Courville, P., Bergevin, I., and Cellier, M. F. (2003) Horizontal gene transfer of "prototype" Nramp in bacteria. *J. Mol. Evol. 57*, 363–376.

(71) Moore, R. B., Obornik, M., Janouskovec, J., Chrudimsky, T., Vancova, M., Green, D. H., Wright, S. W., Davies, N. W., Bolch, C. J., Heimann, K., Slapeta, J., Hoegh-Guldberg, O., Logsdon, J. M., and Carter, D. A. (2008) A photosynthetic alveolate closely related to apicomplexan parasites. *Nature 451*, 959–963.

(72) Nash, E. A., Nisbet, R. E., Barbrook, A. C., and Howe, C. J. (2008) Dinoflagellates: A mitochondrial genome all at sea. *Trends Genet. 24*, 328–335.
(73) Sanchez-Puerta, M. V., and Delwiche, C. F. (2008) A hypothesis for plastid evolution in chromoalveolates. *J. Phycol. 44*, 1097–1107.
(74) Cohen, A., Nevo, Y., and Nelson, N. (2003) The first external loop of the metal ion transporter DCT1 is involved in metal ion binding and specificity. *Proc. Natl. Acad. Sci. U.S.A. 100*, 10694–10699.
(75) Sacher, A., Cohen, A., and Nelson, N. (2001) Properties of the mammalian and yeast metal-ion transporters DCT1 and Smf1p expressed in *Xenopus laevis* oocytes. *J. Exp. Biol. 204*, 1053–1061.
(76) Durr, G., Strayle, J., Plemper, R., Elbs, S., Klee, S. K., Catty, P., Wolf, D. H., and Rudolph, H. K. (1998) The medial-Golgi ion pump Pmr1 supplies the yeast secretory pathway with Ca^{2+} and Mn^{2+} required for glycosylation, sorting, and endoplasmic reticulum-associated protein degradation. *Mol. Biol. Cell 9*, 1149–1162.
(77) Papp-Wallace, K. M., and Maguire, M. E. (2006) Manganese transport and the role of manganese in virulence. *Annu. Rev. Microbiol. 60*, 187–209.
(78) Garrick, M. D., Singleton, S. T., Vargas, F., Kuo, H. C., Zhao, L., Knopfel, M., Davidson, T., Costa, M., Paradkar, P., Roth, J. A., and Garrick, L. M. (2006) DMT1: Which metals does it transport? *Biol. Res. 39*, 79–85.
(79) Cailliatte, R., Schikora, A., Briat, J. F., Mari, S., and Curie, C. (2010) High-affinity manganese uptake by the metal transporter NRAMP1 is essential for *Arabidopsis* growth in low manganese conditions. *Plant Cell 22*, 904–917.
(80) Xiao, S., Li, J., Wang, Y., Wang, C., Xue, R., Wang, S., and Li, F. (2010) Identification of an "α-helix-extended segment-α-helix" conformation of the sixth transmembrane domain in DMT1. *Biochim. Biophys. Acta 1798*, 1556–1564.
(81) Lam-Yuk-Tseung, S., Govoni, G., Forbes, J., and Gros, P. (2003) Iron transport by Nramp2/DMT1: pH regulation of transport by 2 histidines in transmembrane domain 6. *Blood 101*, 3699–3707.
(82) Carpenter, M. L., and Cande, W. Z. (2009) Using morpholinos for gene knockdown in *Giardia intestinalis*. *Eukaryotic Cell 8*, 916–919.
(83) Nicholas, K. B., and Nicholas, H. B. (1997) GeneDoc: A tool for editing and annotating multiple sequence alignments. http://www.nrbsc.org/gfx/genedoc/ (distributed by the authors).
(84) Takezaki, N., Rzhetsky, A., and Nei, M. (2004) Phylogenetic test of the molecular clock and linearized trees. *Mol. Biol. Evol. 12*, 823–833.
(85) Tajima, F., and Nei, M. (1984) Estimation of evolutionary distance between nucleotide sequences. *Mol. Biol. Evol. 1*, 269–285.